blood®
Regular Article

HEMATOPOIESIS AND STEM CELLS

Retinoid X receptor promotes hematopoietic stem cell fitness and quiescence and preserves hematopoietic homeostasis

María Piedad Menéndez-Gutiérrez,[1,*] Jesús Porcuna,[1,*] Ramesh Nayak,[2-4] Ana Paredes,[1] Haixia Niu,[2,3] Vanessa Núñez,[1] Aditi Paranjpe,[3,5] Manuel J. Gómez,[6] Anukana Bhattacharjee,[3,5] Daniel J. Schnell,[3,5] Fátima Sánchez-Cabo,[6] John S. Welch,[7] Nathan Salomonis,[3,5] Jose A. Cancelas,[2-4] and Mercedes Ricote[1]

[1]Centro Nacional de Investigaciones Cardiovasculares, Madrid, Spain; [2]Stem Cell Program, Division of Experimental Hematology and Cancer Biology, Cincinnati Children's Hospital Medical Center, Cincinnati, OH; [3]Department of Pediatrics and [4]Hoxworth Blood Center, University of Cincinnati College of Medicine, Cincinnati, OH; [5]Division of Biomedical Informatics, Cincinnati Children's Hospital Medical Center, Cincinnati, OH; [6]Bioinformatics Unit, Centro Nacional de Investigaciones Cardiovasculares, Madrid, Spain; and [7]Department of Internal Medicine, Washington University, St Louis, MO

KEY POINTS

- **RXRs are ligand-activated transcriptional units needed for the maintenance of HSC fitness, and preservation of a balanced hematopoiesis.**
- **RXRα;RXRβ-deficient HSCs transition from a dormant to a transcriptionally and proliferative-active state through MYC pathway activation.**

Hematopoietic stem cells (HSCs) balance self-renewal and differentiation to maintain hematopoietic fitness throughout life. In steady-state conditions, HSC exhaustion is prevented by the maintenance of most HSCs in a quiescent state, with cells entering the cell cycle only occasionally. HSC quiescence is regulated by retinoid and fatty-acid ligands of transcriptional factors of the nuclear retinoid X receptor (RXR) family. Herein, we show that dual deficiency for hematopoietic RXRα and RXRβ induces HSC exhaustion, myeloid cell/megakaryocyte differentiation, and myeloproliferative-like disease. RXRα and RXRβ maintain HSC quiescence, survival, and chromatin compaction; moreover, transcriptome changes in RXRα;RXRβ-deficient HSCs include premature acquisition of an aging-like HSC signature, MYC pathway upregulation, and RNA intron retention. Fitness loss and associated RNA transcriptome and splicing alterations in RXRα;RXRβ-deficient HSCs are prevented by *Myc* haploinsufficiency. Our study reveals the critical importance of RXRs for the maintenance of HSC fitness and their protection from premature aging.

Introduction

Hematopoietic stem cell (HSC) self-renewal and differentiation are subject to tight transcriptional regulation.[1] Features, such as altered transcriptional programs, cellular stress, or age, can impair HSC fitness and performance.[2,3] HSC fitness loss and exhaustion are associated with a gradual decline in HSC regenerative capacity, leading to an expansion of functionally weakened HSCs with an altered multilineage differentiation potential.[4,5]

Retinoid X receptors (RXRs) are members of the nuclear receptor (NR) superfamily of ligand-dependent transcription factors (TFs)[6] that respond to vitamin A derivatives (retinoids) and some endogenous fatty acids (FAs).[7] RXRs are encoded by 3 genes, *Rxra* (NR2B1), *Rxrb* (NR2B2), and *Rxrg* (NR2B3), which show time-specific and tissue-dependent differential expression. RXRs control pleiotropic genetic programs, such as cell proliferation and differentiation, immune functions, and lipid and glucose metabolism, by forming homodimers and heterodimers with others NRs, including other retinoid-activated receptors, the retinoic acid receptors (RARs).[6] Retinoid-activated receptors are an attractive therapeutic target because of their ability to induce neutrophil differentiation.[8-10] However, their specific role in HSC maintenance and survival remains controversial, with conflicting results obtained with mice vs human HSCs.[10-13] Recent studies with retinoid-supplementation and retinoid-deprivation models demonstrated that retinoid signaling is essential for the regulation of HSC dormancy.[5,14] Because retinoids activate both the RARs and RXRs, some of the effects observed in these studies are likely driven by RXRs. Pharmacologic approaches using RXR ligands suggest the importance of RXRs in HSC self-renewal and myeloid differentiation in vitro,[15,16] although off-target effects and the inability to generate complete loss-of-function models have hampered the interpretation of these

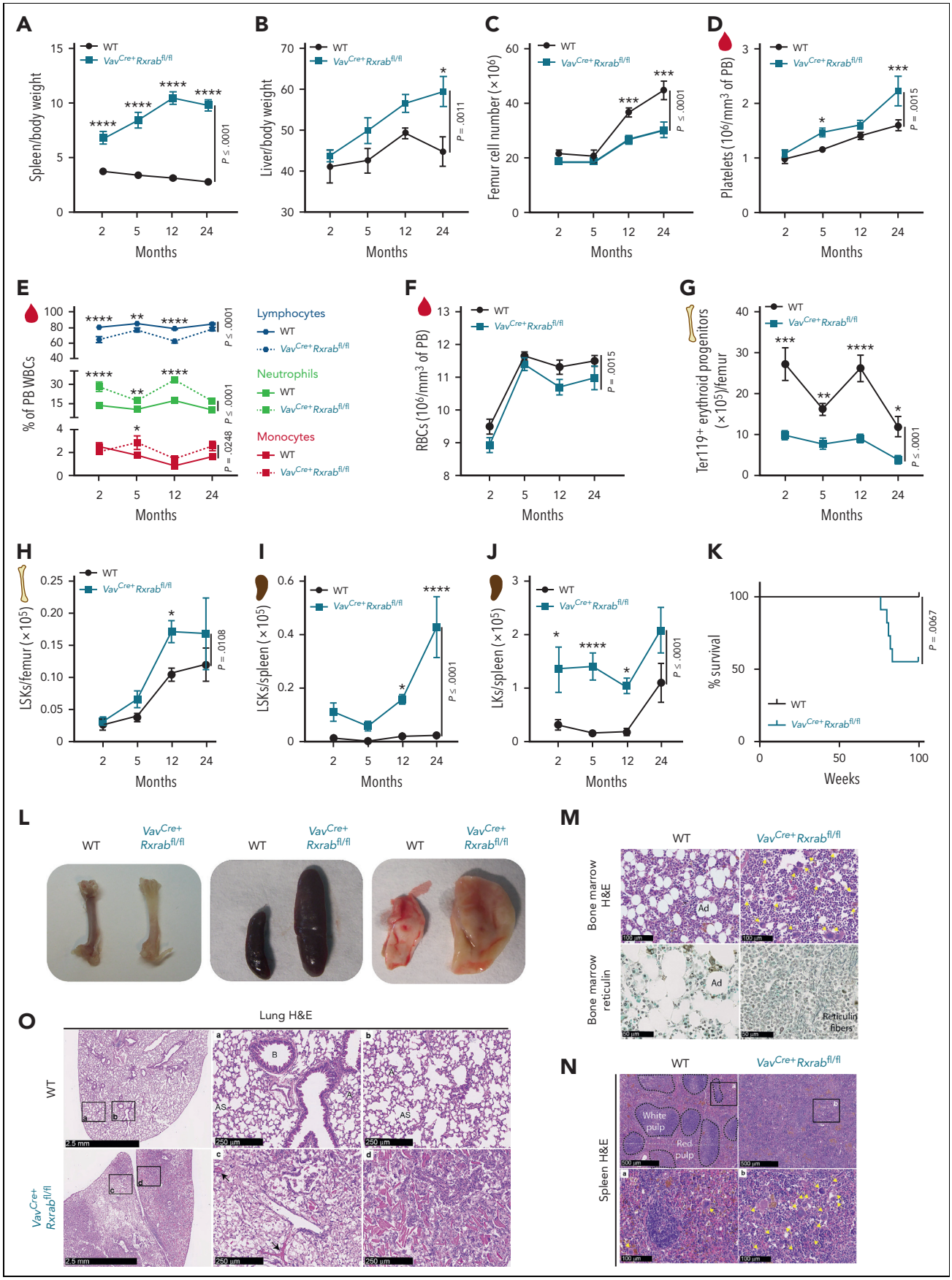
A
Spleen/body weight
WT
Vav^Cre+ Rxrab^fl/fl
Months
P ≤ .0001
B
Liver/body weight
P = .0011
C
Femur cell number (×10^6)
P ≤ .0001
D
Platelets (10^6/mm^3 of PB)
P = .0015
E
% of PB WBCs
Lymphocytes
Neutrophils
Monocytes
P ≤ .0001
P = .0248
F
RBCs (10^6/mm^3 of PB)
P = .0015
G
Ter119+ erythroid progenitors (×10^5)/femur
P ≤ .0001
H
LSKs/femur (×10^5)
P = .0108
I
LSKs/spleen (×10^5)
P ≤ .0001
J
LKs/spleen (×10^5)
P ≤ .0001
K
% survival
Weeks
P = .0067
L
M
Bone marrow H&E
Bone marrow reticulin
Ad
Reticulin fibers
N
Spleen H&E
White pulp
Red pulp
O
Lung H&E
AS
B
A

Figure 1.

experiments. To date, no definitive genetic evidence has confirmed the role of the RXRs in HSC activity, because deficiency of individual RXR isoforms results in compensatory activity.[17] Herein, we demonstrate that double deletion of *Rxra* and *Rxrb* leads to a decline in HSC fitness, characterized by HSC proliferative activation and exhaustion, and concomitant development of myeloproliferative-like disease (MPD). This phenotype derives from loss of HSC quiescence and self-renewal, openness of HSC chromatin, aberrant splicing with increased intron retention, and activation of the signaling pathway controlled by MYC.[18] Using a model of *Myc* haploinsufficiency, we demonstrate that the loss of quiescence and altered transcription and splicing in RXR-deficient HSCs are mediated by MYC pathway activation. Our results provide definitive evidence that RXRs regulate HSC fitness and lineage fate by preserving transcriptional repression of the self-renewal master regulator MYC, and open new perspectives on the development of therapeutic approaches to prevent or reverse loss of HSC fitness.

Materials and methods

Mice

Details of the generation and crossings of the animals used are provided in supplemental Materials and Methods, available on the *Blood* website.

Cell isolation

Cell isolation procedures are detailed in supplemental Materials and Methods.

Flow cytometry and cell sorting

Procedures for flow cytometry and cell sorting are described in supplemental Materials and Methods.

Colony-forming unit cell assays

Colony-forming unit (CFU) cell assays were performed as detailed in supplemental Materials and Methods.

OP9NL1 cocultures

OP9NL1 cocultures were performed as detailed in supplemental Materials and Methods.

Generation of hematopoietic chimeras

Hematopoietic chimeras were generated as detailed in supplemental Materials and Methods.

Homing assays

The procedures for homing assays are detailed in supplemental Materials and Methods.

5-Fluorouracil assay

The 5-fluorouracil (5-FU) assays were performed as detailed in supplemental Materials and Methods.

Immunohistochemistry

Immunohistochemistry approaches are detailed in supplemental Materials and Methods.

HSC first division fate analysis

The procedures for first division fate analysis are described in supplemental Materials and Methods.

Quantitative real-time polymerase chain reaction

Quantitative real-time polymerase chain reaction experiments were performed as detailed in supplemental Materials and Methods.

Single-cell RNA-sequencing processing and analysis

The 10× Genomics Chromium 3′ v2 assay standard protocols were as previously described,[19] with minor modifications detailed in supplemental Materials and Methods.

Bulk, deep RNA-sequencing processing and analysis

Bulk, deep RNA-sequencing assays are detailed in supplemental Materials and Methods.

Chromatin profiling by assay for transposase-accessible chromatin with sequencing

Assay for transposase-accessible chromatin with sequencing was done as previously described,[20] with minor modifications detailed in supplemental Materials and Methods.

Cleavage under target and release using nuclease sequencing assay

Cleavage under target and release using nuclease sequencing (CUT&RUNseq) assays were performed following published methods[21] with minor modifications, as detailed in supplemental Materials and Methods.

Figure 1. $Vav^{Cre+}Rxrab^{fl/fl}$ mice develop lethal myeloproliferative disorders. (A-C) Organ weight and counts of 2-, 5-, 12-, and 24-month-old WT and $Vav^{Cre+}Rxrab^{fl/fl}$ mice. (A-B) Spleen and liver weigh/body weight ratios. (C) BM cellularity per femur. (D-F) Hemogram data of 2-, 5-, 12-, and 24-month-old WT and $Vav^{Cre+}Rxrab^{fl/fl}$ mice. (D) Mean platelet counts. (E) Percentage of lymphocytes, neutrophils, and monocytes among white blood cells (WBCs). (F) Total red blood cells (RBCs). (G-J) Flow cytometry of femur and spleen homogenates from 2-, 5-, 12-, and 24-month-old WT and $Vav^{Cre+}Rxrab^{fl/fl}$ mice. (G) Absolute numbers of erythroid progenitors ($CD45^{-}Ter119^{+}$ cells) per femur. (H) Absolute numbers of LSKs per femur. (I-J) Absolute numbers of spleen LSKs and LKs. (K) Kaplan-Meier survival plots for WT and $Vav^{Cre+}Rxrab^{fl/fl}$ mice (n = 11-13 per genotype). (L) Representative images of femurs, spleens, and lungs of 24-month-old WT and $Vav^{Cre+}Rxrab^{fl/fl}$ mice. (M-N) Representative images of hematoxylin and eosin (H&E)– and reticulin-stained femur sections, and of H&E-stained spleen sections from 24-month-old WT and $Vav^{Cre+}Rxrab^{fl/fl}$ mice; yellow arrows indicate megakaryocytes. Scale bars: 500 μm (N, upper panels), 100 μm (M, upper panels; N, bottom panels), or 50 μm (M, bottom panels). (O) Representative images of H&E-stained lungs from 24-month-old WT and $Vav^{Cre+}Rxrab^{fl/fl}$ mice; black arrows indicate alveolar hemorrhage. Scale bars: 2.5 mm (left panels) or 250 μm (middle and right panels). Data are presented as mean ± SEM: (A-F) n = 7 to 17 mice, pooled from up to 3 independent experiments per age group and genotype; (G) n = 3 to 13 mice, pooled from up to 2 independent experiments per age group and genotype; (H) n = 4 to 24 mice, pooled from up to 3 independent experiments per age group and genotype; (I) n = 5 to 12, pooled from up to 2 independent experiments per age and genotype (spleen); (J) n = 5 to 11 mice, pooled from up to 2 independent experiments per age and genotype. Significance was determined by 2-way analysis of variance followed by the Sidak multiple comparisons test (age-paired mice) (A-J) or log-rank (Mantel-Cox) test (K), and is represented as follows: $*P \le .05$, $**P \le .01$, $***P \le .001$, and $****P \le .0001$. A, alveoli; Ad, adipocytes; AS, alveolar sac; B, bronchiole.

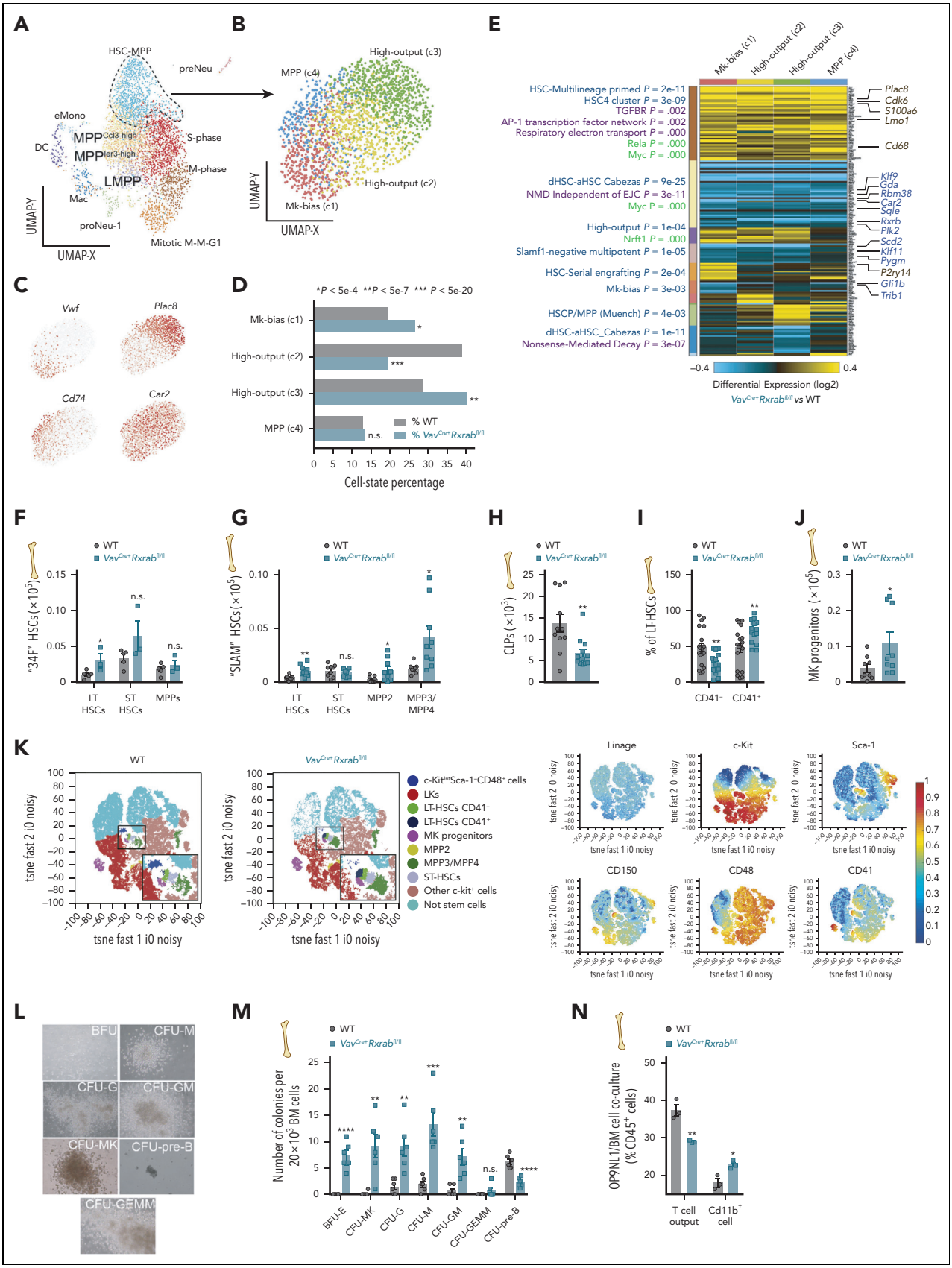
A
HSC-MPP
preNeu
eMono
DC
MPPCcl3-high
MPPIer3-high
S-phase
M-phase
LMPP
Mac
proNeu-1
Mitotic M-M-G1
UMAP-Y
UMAP-X
B
High-output (c3)
MPP (c4)
High-output (c2)
Mk-bias (c1)
UMAP-Y
UMAP-X
E
Mk-bias (c1)
High-output (c2)
High-output (c3)
MPP (c4)
HSC-Multilineage primed P = 2e-11
HSC4 cluster P = 3e-09
TGFBR P = .002
AP-1 transcription factor network P = .002
Respiratory electron transport P = .000
Rela P = .000
Myc P = .000
dHSC-aHSC Cabezas P = 9e-25
NMD Independent of EJC P = 3e-11
Myc P = .000
High-output P = 1e-04
Nrft1 P = .000
Slamf1-negative multipotent P = 1e-05
HSC-Serial engrafting P = 2e-04
Mk-bias P = 3e-03
HSCP/MPP (Muench) P = 4e-03
dHSC-aHSC_Cabezas P = 1e-11
Nonsense-Mediated Decay P = 3e-07
Plac8
Cdk6
S100a6
Lmo1
Cd68
Klf9
Gda
Rbm38
Car2
Sqle
Rxrb
Plk2
Scd2
Klf11
Pygm
P2ry14
Gfi1b
Trib1
–0.4
0.4
Differential Expression (log2)
Vav^Cre+Rxrab^fl/fl vs WT
C
Vwf
Plac8
Cd74
Car2
D
*P < 5e-4 **P < 5e-7 *** P < 5e-20
Mk-bias (c1)
High-output (c2)
High-output (c3)
MPP (c4)
% WT
% Vav^Cre+Rxrab^fl/fl
n.s.
0 5 10 15 20 25 30 35 40
Cell-state percentage
F
WT
Vav^Cre+Rxrab^fl/fl
"34F" HSCs (×10^5)
LT HSCs
ST HSCs
MPPs
G
WT
Vav^Cre+Rxrab^fl/fl
"SLAM" HSCs (×10^5)
LT HSCs
ST HSCs
MPP2
MPP3/ MPP4
H
WT
Vav^Cre+Rxrab^fl/fl
CLPs (×10^3)
I
WT
Vav^Cre+Rxrab^fl/fl
% of LT-HSCs
CD41⁻
CD41⁺
J
WT
Vav^Cre+Rxrab^fl/fl
MK progenitors (×10^5)
K
WT
Vav^Cre+Rxrab^fl/fl
tsne fast 2 i0 noisy
tsne fast 1 i0 noisy
c-Kit^int Sca-1⁻CD48⁺ cells
LKs
LT-HSCs CD41⁻
LT-HSCs CD41⁺
MK progenitors
MPP2
MPP3/MPP4
ST-HSCs
Other c-kit⁺ cells
Not stem cells
Linage
c-Kit
Sca-1
CD150
CD48
CD41
L
BFU
CFU-M
CFU-G
CFU-GM
CFU-MK
CFU-pre-B
CFU-GEMM
M
WT
Vav^Cre+Rxrab^fl/fl
Number of colonies per 20×10^3 BM cells
BFU-E
CFU-MK
CFU-G
CFU-M
CFU-GM
CFU-GEMM
CFU-pre-B
N
WT
Vav^Cre+Rxrab^fl/fl
OP9NL1/BM cell co-culture (% CD45⁺ cells)
T cell output
Cd11b⁺ cell

Figure 2.

Serial competitive repopulation of *Myc* haploinsufficient HSCs

Serial competitive repopulation assays are described in supplemental Materials and Methods.

Statistical analysis

Statistical procedures are described in supplemental Materials and Methods.

Results

Dual deletion of RXRα and RXRβ in the hematopoietic compartment causes expansion of the multipotential and myeloid progenitor cell pools

Transcript expression analysis of bone marrow (BM) hematopoietic cell subsets revealed ubiquitous *Rxra* and *Rxrb* expression in hematopoietic stem and multipotential progenitor cells (HSC/Ps; lineage$^-$Sca-1$^+$c-kit$^+$ cells; LSKs), including long-term (LT) HSCs, short-term HSCs, and multipotent progenitors (MPP2 and MPP3/MPP4),[22] as well as in committed erythromyeloid progenitors (lineage$^-$Sca-1$^-$c-kit$^+$ cells; LKs), including common myeloid, granulocyte-monocyte, and erythroid-megakaryocyte progenitors (supplemental Figure 1A-B). In all these hematopoietic populations, *Rxrg* expression was undetectable (qPCR cycle threshold [C_T] values ≥35). We inactivated RXRα or RXRβ in the HSC/Ps of neonatal polyinosinic:polycytidylic acid (pI:pC)-inducible Mx-1^{Cre} transgenic mice[23] (supplemental Figure 2A). Postnatal deletion of RXRα (*Mx-1*$^{Cre+}$*Rxra*$^{fl/fl}$ mice) or RXRβ (*Mx-1*$^{Cre+}$*Rxrb*$^{fl/fl}$ mice) in HSC/Ps was insufficient to substantially alter hematopoiesis (supplemental Figure 2B-G; supplemental Table 1). However, the deletion of both RXR isoforms (*Mx-1*$^{Cre+}$*Rxrab*$^{fl/fl}$ mice) led to paler bones, reduced BM cellularity, splenomegaly, T-cell lymphopenia, and neutrophilia (supplemental Figure 2A-B; supplemental Table S1). *Mx-1*$^{Cre+}$*Rxrab*$^{fl/fl}$ mice also had significantly elevated numbers of eosinophils and LSKs in BM, reduced T-cell numbers in peripheral blood (PB) and spleen, and significantly elevated numbers of spleen LSKs, LKs, and mature myeloid cells (supplemental Figure 2C-G). Thus, lack of RXRα;RXRβ in HSC/Ps leads to an expansion of multipotential and myeloid progenitor populations and to lymphopenia.

RXRα;RXRβ-deficient mice develop fatal myeloproliferative disease, featuring prominent extramedullary hematopoiesis

To specifically delete *Rxra* and *Rxrb* in the hematopoietic compartment from embryonic stages onwards, we used the pan-hematopoietic Vav^{Cre} mouse model.[24] This resulted in loss of *Rxra* and *Rxrb* expression in HSC/Ps (supplemental Figure 3A) with no compensatory upregulation of *Rxrg* (C_T values ≥ 35). Analysis of hematopoietic parameters over 2 years revealed extramedullary hematopoiesis in *Vav*$^{Cre+}$*Rxrab*$^{fl/fl}$ mice, shown by an early increase in spleen/body weight ratio, a progressive increase in liver/body weight ratio, and a later reduction in BM cellularity (Figure 1A-C; supplemental Figure 3B). PB analysis of young *Vav*$^{Cre+}$*Rxrab*$^{fl/fl}$ mice revealed thrombocytosis (Figure 1D), lymphocytopenia, neutrophilia, and monocytosis (Figure 1E), as well as mild microcytic anemia (Figure 1F; supplemental Figure 3C) and reduced BM erythropoiesis (Figure 1G; supplemental Figure 3D-E). *Vav*$^{Cre+}$*Rxrab*$^{fl/fl}$ mice also had significantly increased numbers of BM and spleen LSKs (Figure 1H-I) and of spleen LKs, neutrophils, eosinophils, and monocytes (Figure 1J; supplemental Figure 3F-H). These animals also showed a significant reduction in the numbers of PB B and T lymphocytes and in the CD4:CD8 ratio (supplemental Figure 3I-J). All these hematopoietic alterations persisted, and in most cases were magnified in aged *Vav*$^{Cre+}$*Rxrab*$^{fl/fl}$ mice (Figure 1A-J; supplemental Figure 3C-J). Approximately half of the *Vav*$^{Cre+}$*Rxrab*$^{fl/fl}$ mice died at around 80 weeks of age, whereas none of the wild-type (WT) mice had died at the study end point (Figure 1K). Necropsy of surviving 24-month-old *Vav*$^{Cre+}$*Rxrab*$^{fl/fl}$ mice revealed pale bones, pronounced splenomegaly, and enlarged yellow-milky lungs (Figure 1L). Histologic studies of distal femurs revealed increased numbers of megakaryocytes with hyperlobulated nuclei and an absence of adipocytes, with 50% of *Vav*$^{Cre+}$*Rxrab*$^{fl/fl}$ mice also presenting increased reticulin fibrosis with no collagen deposition (Figure 1M; supplemental Figure 4A). *Vav*$^{Cre+}$*Rxrab*$^{fl/fl}$ mice had enlarged spleens with altered architecture and increased numbers of megakaryocytes (Figure 1L,N), as well as an overabundance of liver and lung leukocytes (Figure 1O; supplemental Figure 4B-D). Histopathologic changes in *Vav*$^{Cre+}$*Rxrab*$^{fl/fl}$ lung tissue included massive alveolar inflammatory infiltration, accumulation of lipid-laden cells, alveolar hemorrhage, and abundant crystal deposition (Figure 1O).

Figure 2. Expansion of megakaryocyte–myeloid-biased stem cells in RXRα;RXRβ-deficient mice. (A-E) Single-cell RNA sequencing (10× Genomics) of sorted LSKs from WT and *Vav*$^{Cre+}$*Rxrab*$^{fl/fl}$ BM cells (shown are clusters derived from gene set enrichment of a compendium of prior HSC/P subsets from single-cell functional studies).[27] (A-B) UMAP plots of HSC/P subsets derived from *Vav*$^{Cre+}$*Rxrab*$^{fl/fl}$ and WT BM LSKs (A), and of subclustering of the broader HSC-MPP cluster (B). (C) Top HSC-MPP cluster marker genes. (D) HSC-MPP population frequencies, showing significant differences between *Vav*$^{Cre+}$*Rxrab*$^{fl/fl}$ and WT mice (Fischer exact *P*-value thresholds are indicated). (E) Heat map showing differentially expressed genes identified by cellHarmony analysis of each HSC-MPP subcluster in *Vav*$^{Cre+}$*Rxrab*$^{fl/fl}$ vs WT mice. On the left of the associated clusters are shown enriched prior-defined HSC/P functional subsets (blue), pathways (purple), or curated transcription factor targets (green) (GO-Elite software); on the right of the associated clusters are shown matching bulk RNA-seq regulated genes. (F-K) Flow cytometry of BM from 5-month-old WT and *Vav*$^{Cre+}$*Rxrab*$^{fl/fl}$ mice. (F-G) Absolute numbers of HSC subpopulations per femur, according to the "34F" or "SLAM" stain codes. (H) Absolute numbers of common lymphoid progenitors (CLPs) per femur. (I) Frequency of CD41$^+$ and CD41$^-$ cells in the CD150$^+$CD48$^-$ LT-HSC subset. (J) Absolute numbers of MK progenitor per femur. (K) Annotated t-SNE plots for the identified lineage$^-$ BM-cell populations from WT and *Vav*$^{Cre+}$*Rxrab*$^{fl/fl}$ mice using the "SLAM" stain code as in G. Insets in the left panels show magnifications of the plotted HSC/P subpopulations; plots in the right panels show overlaid biexponential transformed marker expression levels (n = 3-4 per genotype). (L-M) Colony-forming unit (CFU) assay in total BM cells from 5-month-old WT and *Vav*$^{Cre+}$*Rxrab*$^{fl/fl}$ mice. (L) Representative images of hematopoietic colonies identified in *Vav*$^{Cre+}$*Rxrab*$^{fl/fl}$ mice after 7 days of incubation: burst-forming unit-erythroid (BFU), unipotent CFU-M (monocyte), CFU-MK (megakaryocyte), CFU-G (granulocyte), and CFU–pre-B (B lymphocyte) progenitors; bipotent CFU-GM (granulocyte, monocyte) progenitors; and multipotent CFU-GEMM (granulocyte, erythrocyte, monocyte, and megakaryocyte) progenitors. (M) Number of colonies per 20 × 10^3 plated BM cells (n = 6; 3 mice per genotype, with 2 technical replicates per mouse; data are representative of 2 independent experiments). (N) Lymphocyte output after 8 days of OP9NL1 cell coculture with BM cells from 5-month-old WT and *Vav*$^{Cre+}$*Rxrab*$^{fl/fl}$ mice; graph shows the percentage of T cells (DN1 + DN2 + DN3 + DN4 + CD3$^+$ cells; for gating strategy, see supplemental Figure 6F) and Cd11b$^+$ cells within CD45$^+$ lymphocytes. Data are shown as means ± SEM, and dots represent individual animals. Significance was determined by unpaired Student *t* test, and is represented as follows: *$P \le .05$, **$P \le .01$, ***$P \le .001$, and ****$P \le .0001$. n.s., not significant.

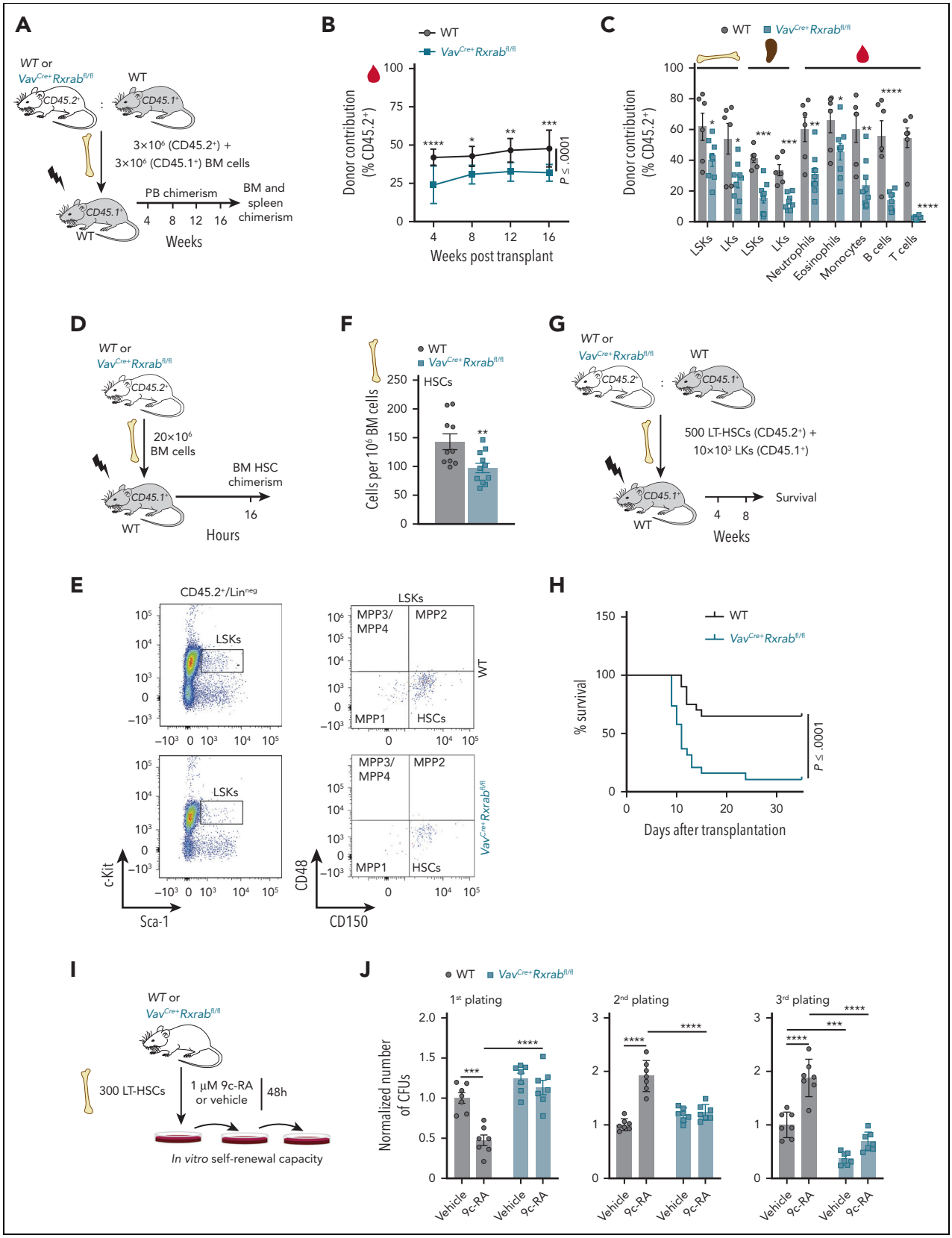

Figure 3. RXRα;RXRβ-deficient HSCs are functionally defective. (A-C) Competitive transplantation assay (1:1 mix) of unfractionated BM cells from WT or *Vav*$^{Cre+}$*Rxrab*$^{fl/fl}$ mice (CD45.2$^+$) and C57BL/6 mice (CD45.1$^+$) into lethally irradiated C57BL/6 mice (CD45.1$^+$) (data are representative of 3 independent experiments). (A) Experimental design. (B) Fluorescence-activated cell sorting (FACS) analysis of the percentage of total donor chimerism in PB 4, 8, 12, and 16 weeks after transplantation (n = 9-10). (C) FACS analysis of cell-specific chimerism in PB, BM, and spleen 16 weeks after competitive repopulation assay. (D-F) Homing assay of total BM cells from WT or *Vav*$^{Cre+}$*Rxrab*$^{fl/fl}$ mice (CD45.2$^+$), transplanted into lethally irradiated C57BL/6 mice (CD45.1$^+$). (D) Experimental design. (E) Representative FACS plots showing the gating strategies for analysis of

Morphologic analysis of PB smears showed no detectable blasts, immature myeloblasts, or erythroid precursors in $Vav^{Cre+}Rxrab^{fl/fl}$ mice. The histopathologic data of $Vav^{Cre+}Rxrab^{fl/fl}$ marrow and extramedullary hematopoiesis fulfilled the criteria for murine MPD.[25,26]

RXRα;RXRβ-deficient HSCs show myeloid-megakaryocyte skewing and impaired repopulating activity

Single-cell RNA-sequencing analysis of sorted BM LSKs identified 12 shared discrete prior-defined cell states,[27] including presumptive HSC-MPP and MPP in distinct cell-cycle phases (Figure 2A; supplemental Figure 5A-B). $Vav^{Cre+}Rxrab^{fl/fl}$ LSKs were enriched in mitotic M-M-G1, eMono, proNeu-1, and LMPP clusters, whereas WT LSKs showed enrichment in the $MPP^{Ier3\text{-}high}$ and HSC-MPP clusters (GO-Elite Fischer Exact $P \leq 10^4$) (supplemental Figure 5C). Subclustering of the HSC-MPP cluster detected 4 subsets, 2 of them enriched in $Vav^{Cre+}Rxrab^{fl/fl}$ cells: (a) *Vwf*-enriched megakaryocyte-biased activated, cycling HSCs (c1)[28] and (b) high-output cells corresponding to proliferative *Plac8*-expressing LT-HSCs (c3)[29,30] (Figure 2B-D). In contrast, WT HSC-MPPs were enriched in *Car2*-positive high-output MPPs (c2)[27] (Figure 2B-D). Gene set enrichment analysis of the 4 HSC-MPP subclusters identified enriched gene sets associated with HSC priming and activation[5,27,31] in $Vav^{Cre+}Rxrab^{fl/fl}$ HSC-MPPs (Figure 2E). All HSC-MPP populations from $Vav^{Cre+}Rxrab^{fl/fl}$ mice showed upregulation of MYC-dependent mRNA transcripts (eg, *Cdk6* and *S100a6*)[32,33] and downregulation of genes associated with nonsense-mediated decay (Figure 2E).

Fluorescence-activated cell sorting analysis of BM LSKs according to the expression of CD34 and the FMS-like tyrosine kinase 3 (FLT3) receptor ("34F" HSCs)[34] and of CD48 and CD150 ("SLAM" HSCs)[22,35] revealed expansion of the most primitive HSC population ($CD34^-FLT3^-$ and $CD150^+CD48^-$ LT-HSCs), myeloid-biased MPPs ($CD150^+CD48^+$ MPP2),[22] and $CD150^-CD48^+$ cells containing both myeloid-biased MPP3[22] and lymphoid-primed MPP4[22] (Figure 2F,G,K; supplemental Figure 6A-C). However, $Vav^{Cre+}Rxrab^{fl/fl}$ BM showed significant depletion of downstream lymphoid-committed progenitors (Figure 2H; supplemental Figure 6D), whereas there was an expansion of $CD41^+$ LT-HSCs (considered primed HSCs that accumulate with age[36] and have short-term—and primarily myeloid—regenerative potential[37]) and megakaryocyte-committed progenitors[38] (Figure 2I-K; supplemental Figure 5H). Consistently, functional assays of BM progenitors revealed a marked increase in the numbers of megakaryocyte/myeloid colony forming units (CFUs), a decrease of pre-B CFUs (Figure 2L-M), and a reduction in stroma-dependent T-cell output (OP9NL1/BM cocultures; Figure 2N; supplemental Figure 6F-G). Analysis of PB CFUs revealed significantly higher numbers of CFU-G (granulocyte) and CFU-GM (granulocyte/monocyte) in $Vav^{Cre+}Rxrab^{fl/fl}$ mice (supplemental Figure 6H-I), suggesting mobilization of myeloid-biased HSCs from BM to secondary hematopoietic organs. These data demonstrate that most expanded HSC/P subsets in $Vav^{Cre+}Rxrab^{fl/fl}$ mice were phenotypic LT-HSCs and myeloid-megakaryocyte progenitors with in vitro colony-forming ability.

We studied the repopulation capacity of WT and $Vav^{Cre+}Rxrab^{fl/fl}$ HSC/Ps, both alone or with a WT competitor[39] (Figure 3A; supplemental Figure 7A). Analysis of PB cell chimerism revealed abnormal repopulation of $Vav^{Cre+}Rxrab^{fl/fl}$ HSC/Ps at each time interval (Figure 3B; supplemental Figure 7B), with an especially marked decline in T-lymphocyte reconstitution (Figure 3C; supplemental Figure 7C). In addition, BM and spleen HSC/P chimerism was significantly diminished when $Vav^{Cre+}Rxrab^{fl/fl}$ BM cells were transplanted with a WT competitor (Figure 3C). We then analyzed the homing capacity of HSCs after intravenous injection of WT or $Vav^{Cre+}Rxrab^{fl/fl}$ BM or $c\text{-}kit^+$ cells into lethally irradiated mice, observing a significantly reduced homing of $Vav^{Cre+}Rxrab^{fl/fl}$ BM progenitors and HSCs (Figure 3D-F; supplemental Figure 7D-F). We analyzed the LT reconstitution capacity of HSCs by serially transferring BM cells through primary and secondary WT recipients. To avoid engraftment defects, we used $Mx\text{-}1^{Cre+}Rxrab^{fl/fl}$ or WT mice as BM donors and induced *Rxra/Rxrb* deletion by intraperitoneal administration of pI:pC at 4 weeks after transplantation (supplemental Figure 7G-H). Although primary recipients had comparable numbers of HSC/Ps regardless of donor genotype (data not shown), secondary recipients of $Mx\text{-}1^{Cre+}Rxrab^{fl/fl}$ BM had significantly fewer HSC/Ps than recipients of WT BM (supplemental Figure 7I). As a more rigorous test of HSC fitness, a limiting number of HSCs from WT *or* $Vav^{Cre+}Rxrab^{fl/fl}$ mice were cotransplanted with supporting WT LKs into irradiated mice (Figure 3G). Of the irradiated animals transplanted with $Vav^{Cre+}Rxrab^{fl/fl}$ HSCs, 90% died after the second week post-transplantation (Figure 3H), indicating that $Vav^{Cre+}Rxrab^{fl/fl}$ HSCs were deprived of hematopoietic radioprotection activity. Accordingly, colony replating assays revealed that $Vav^{Cre+}Rxrab^{fl/fl}$ HSCs lost their self-renewal capacity, whereas activation of RXRs with the retinoid 9c-RA enhanced their replating capacity (Figure 3I-J). These results indicate that RXRs have a cell-autonomous effect on HSC fitness, and that loss of RXRs severely compromises the capacity of HSCs to home and radioprotect.

Quiescent HSCs transition to an active proliferative state in the absence of RXRs

To understand the role of RXRs in HSC/P proliferation, we performed a baseline in vivo 5-bromo-2′-deoxyuridine (BrdU) pulse, demonstrating that $Vav^{Cre+}Rxrab^{fl/fl}$ LSKs and LT-HSCs progress faster than their WT counterparts through the cell-cycle S phase (Figure 4A). Pyronin Y coupled to Hoechst 33342 labeling indicated that $Vav^{Cre+}Rxrab^{fl/fl}$ LSKs and LT-HSCs had higher cell-cycle

Figure 3 (continued) $CD45.2^+$ HSCs. (F) Total numbers of $CD45.2^+$ HSCs found in the BM of recipient mice. (G-H) Transplantation of purified LT-HSCs from WT or $Vav^{Cre+}Rxrab^{fl/fl}$ mice ($CD45.2^+$) along with LKs from C57BL/6 mice ($CD45.1^+$) into lethally irradiated C57BL/6 mice ($CD45.1^+$) (n = 19-20; data pooled from 2 independent experiments). (G) Experimental design. (H) Kaplan-Meier survival plot. (I-J) Serial CFU plating assay after 48-hours in vitro treatment of purified LT-HSCs from 5-month-old WT or $Vav^{Cre+}Rxrab^{fl/fl}$ mice with 9c-RA or vehicle. (I) Experimental design. (J) Number of CFUs normalized to control vehicle treatment of each corresponding plating (data pooled from 2 independent experiments). All data are shown as means ± SEM, and dots represent individual animals. Significance was determined by 2-way analysis of variance (ANOVA) followed by the Sidak multiple comparisons test (B), unpaired Student *t* test (C and F), log-rank (Mantel-Cox) test (H), or ordinary 1-way ANOVA (J), and is represented as follows: $^*P \leq .05$, $^{**}P \leq .01$, $^{***}P \leq .001$, and $^{****}P \leq .0001$.

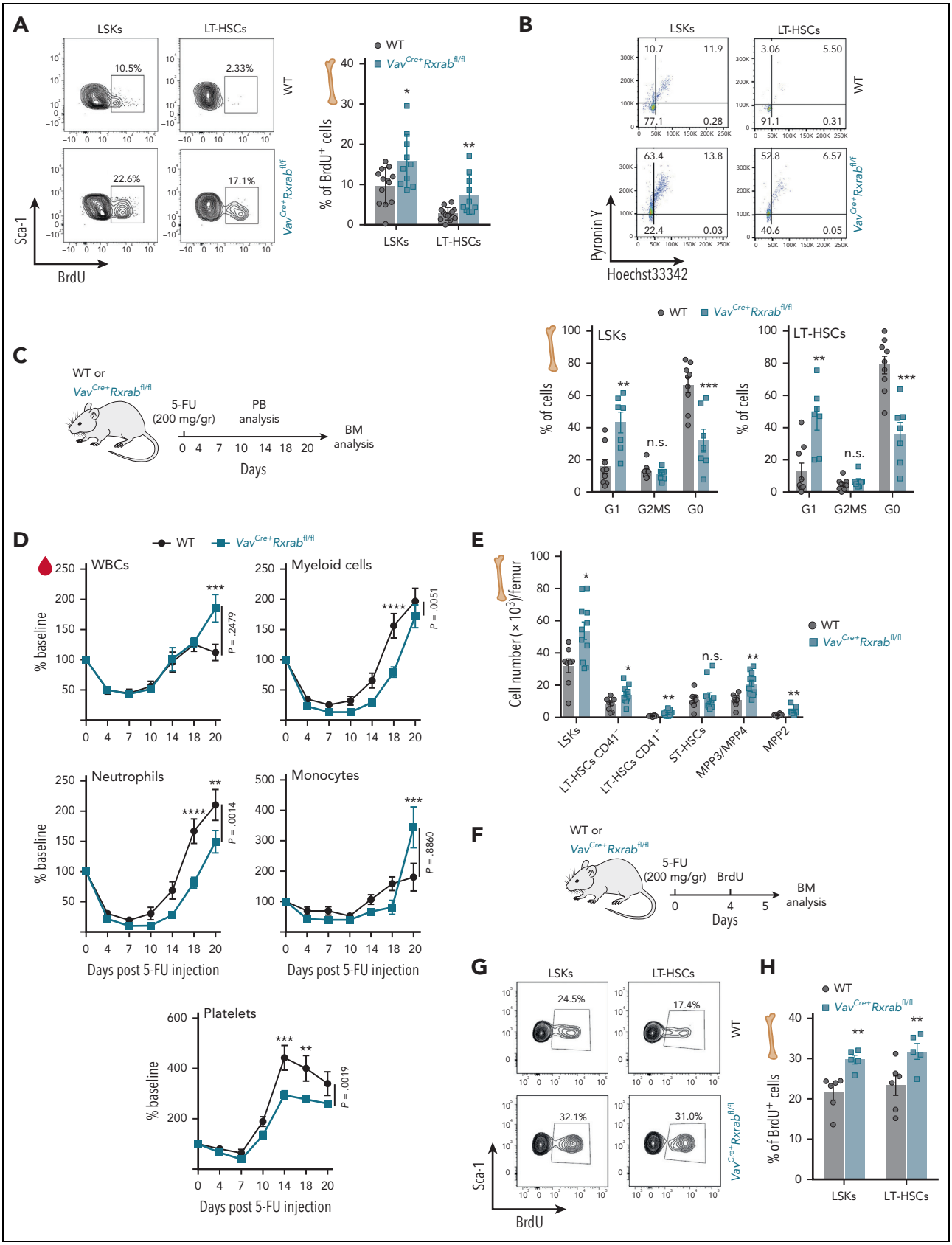

Figure 4. Dual lack of RXRα and RXRβ in HSCs leads to cell-cycle activation and quiescence exit. (A) Representative flow cytometry density plots showing 5-bromo-2′-deoxyuridine (BrdU) incorporation by LSKs and CD150$^+$CD48$^-$ LT-HSCs after a 24-hour pulse (left); the plot (right) shows the frequencies of cells with BrdU incorporation (data are pooled from 2 independent experiments). (B) Representative flow cytometry density plots showing pyronin Y and Hoechst 33342 staining by LSKs and CD150$^+$CD48$^-$ LT-HSCs (upper plots); the lower plots show frequencies of cells with double pyronin Y and Hoechst 33342 staining (data are pooled from 2 independent experiments).

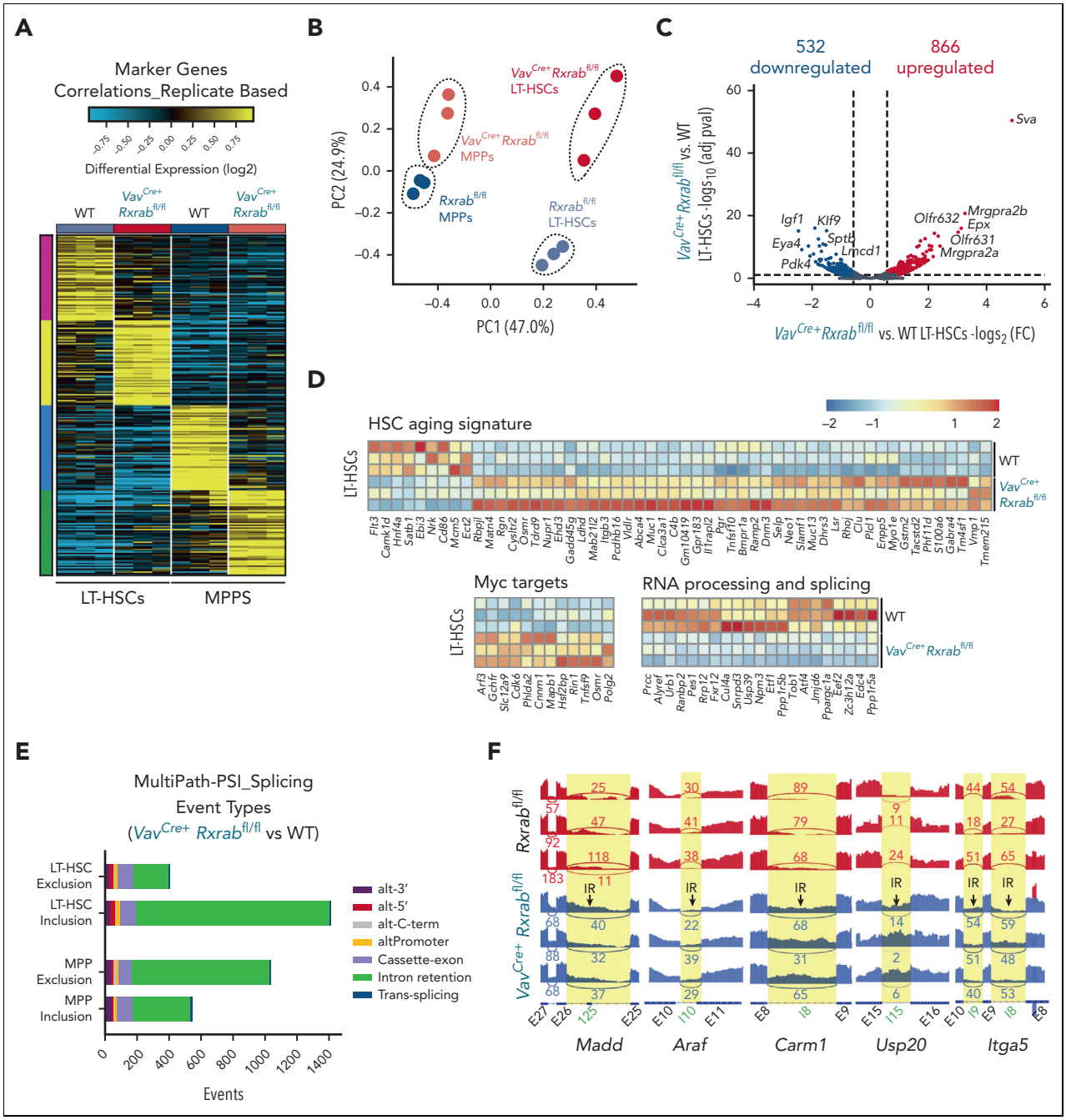

Figure 5.

activity and fewer G_0 phase cells than their WT counterparts, indicating loss of quiescence by RXRα;RXRβ-deficient HSC/Ps (Figure 4B). In addition, annexin-V/4′,6-diamidino-2-phenylindole (DAPI) labeling assays showed reduced frequencies of *Vav-Cre+Rxrab*$^{fl/fl}$ LSKs and LKs entering apoptosis (supplemental Figure 7J-K).

Figure 4 (continued) (C-E) Recovery of hematopoietic cells after 5-fluorouracil (5-FU) administration to *Vav*$^{Cre+}$*Rxrab*$^{fl/fl}$ and WT mice. (C) Experimental design. (D) Time course of PB-cell counts (baseline was defined as the mean reading on day 0, expressed as 100%; n = 9-11 mice per genotype). (E) Absolute HSC/P numbers in total BM 20 days after 5-FU administration. (F-H) HSC/P proliferation 5 days after 5-FU administration to *Vav*$^{Cre+}$*Rxrab*$^{fl/fl}$ and WT mice. (F) Experimental design. (G) Representative flow cytometry density plots showing BrdU incorporation by LSKs and CD150^{+}CD48^{-} LT-HSCs. (H) Frequencies of BrdU-positive cells. All data are presented as means ± SEM, and dots represent individual animals. Significance was determined by unpaired Student *t* test (A, B, E, and H) or 2-way analysis of variance followed by the Sidak multiple comparisons test (D; age-paired mice), and is represented as follows: *$P \le .05$, **$P \le .01$, ***$P \le .001$, and ****$P \le .0001$. n.s., not significant.

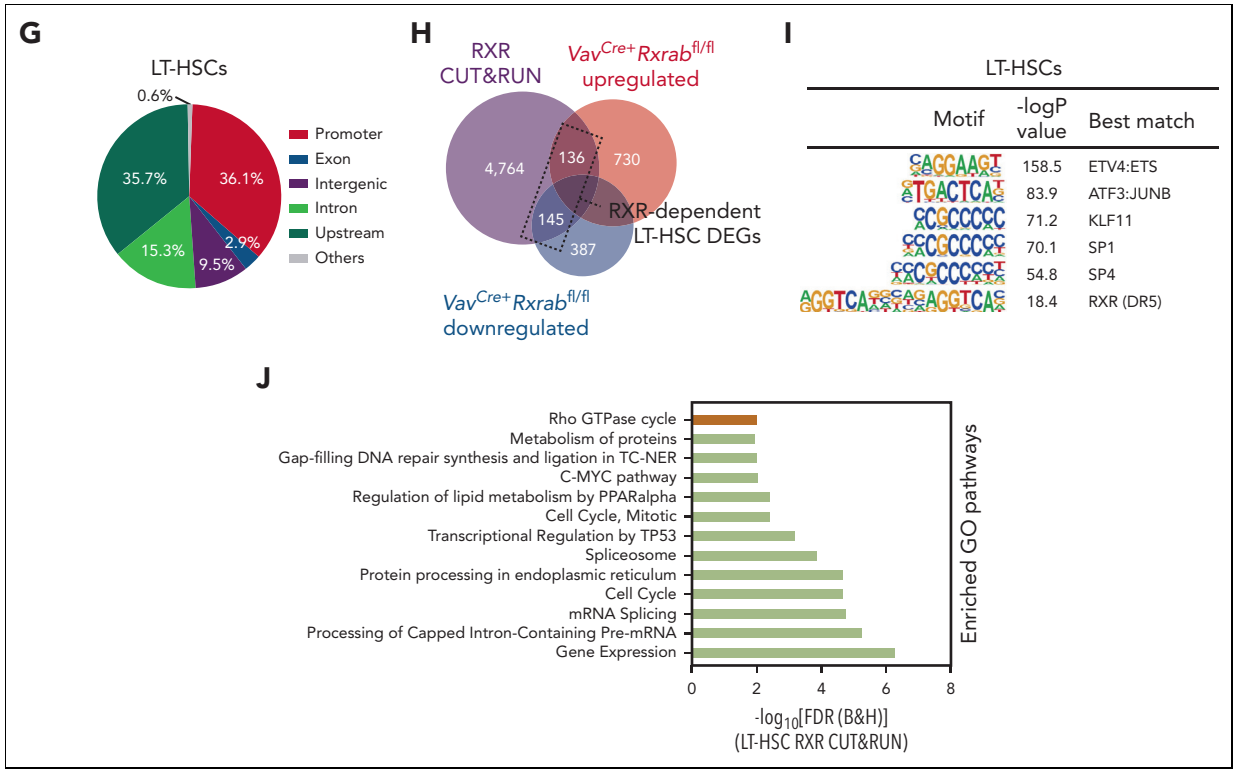

Figure 5 (continued) Lack of RXRα and RXRβ provokes an HSC-aged signature, MYC signaling pathway activation, and intron retention in LT-HSCs. (A-F) Bulk transcriptome of WT and *Vav*$^{Cre+}$*Rxrab*$^{fl/fl}$ LT-HSCs and MPP BM cells. (A) Heat map showing the top specific marker genes per sorted population/genotype, obtained with MarkerFinder software. (B) Principal component (PC) analysis of the transcriptomes in A. (C) Volcano plot showing the global transcriptional changes in *Vav*$^{Cre+}$*Rxrab*$^{fl/fl}$ vs WT LT-HSCs determined by bulk RNA-seq. Each circle represents one differentially expressed gene (DEG), and colored circles represent DEGs showing significant upregulation (adjusted *P* [*P*-adj] ≤ .1 and FC ≥ 1.5 [red]) or significant downregulation (*P*-adj ≤ .1 and FC ≤ −1.5 [blue]). Normalized expression values from bulk RNA-seq data are provided in supplemental Table 2. (D) Heat map showing normalized $\log_2$FC for the expression of HSC aging signature genes, MYC pathway genes, and RNA processing and splicing-related genes in WT and *Vav*$^{Cre+}$*Rxrab*$^{fl/fl}$ LT-HSCs. (E-F) Number of alternative splicing events in *Vav*$^{Cre+}$*Rxrab*$^{fl/fl}$ vs WT LT-HSCs and MPPs for distinct alternative exon and intron usage forms. Splicing events associated with exon or intron inclusion (increased relative expression) vs exclusion are shown separately for LT-HSC and MPP comparisons. (F) SashimiPlot read-level visualization of intron–retention-associated splicing events in WT (red) and *Vav*$^{Cre+}$*Rxrab*$^{fl/fl}$ (blue) bulk RNA-seq LT-HSC samples. Exon-exon junction-spanning reads are denoted with curved lines, together with associated read counts. (G-J) RXRα whole genome binding (CUT&RUNseq). (G) Genomic distribution of enriched regions in WT LT-HSCs identified in the RXR CUT&RUNseq data set. (H) Overlaps of total LT-HSC RXRα CUT&RUNseq peaks with bulk RNA-seq upregulated and dowregulated genes in *Vav*$^{Cre+}$*Rxrab*$^{fl/fl}$ vs WT LT-HSCs. (I) HOMER analysis of known motifs in WT LT-HSC RXRα peaks. (J) List of significantly enriched Gene Ontology (GO) terms in WT LT-HSC promoters (±1 kb from the transcription start site [TSS]; green bars) and upstream regions (±1-20 kb from the TSS; brown bar) for diverse pathways on analysis of the RXRα CUT&RUNseq data set using the Cincinnati Children's Hospital Medical Center (CCHMC) ToppGene suite (https://toppgene.cchmc.org/enrichment.jsp) (false discovery rate [Benjamini and Hochberg (B&H)] ≤ 0.01).

We treated *Vav*$^{Cre+}$*Rxrab*$^{fl/fl}$ and WT mice with 5-fluorouracil (5-FU) and tracked stressed hematopoietic recovery over 20 days (Figure 4C). Early (day 10-18) neutrophil and platelet recoveries were significantly delayed in *Vav*$^{Cre+}$*Rxrab*$^{fl/fl}$ mice (Figure 4D), confirming a fitness deficit in the response of RXRα;RXRβ-deficient HSCs. However, *Vav*$^{Cre+}$*Rxrab*$^{fl/fl}$ myeloid cells showed higher proliferative capacity in the late recovery phase, as shown by a significantly higher rebound than WT on posttreatment days 18 to 20 (2.15 ± 0.75 vs 1.26 ± 0.40 fold change; $P = .0055$), with this effect especially pronounced for monocytes (4.24 ± 2.61 vs 1.14 ± 0.87 fold change; $P = .0034$) (Figure 4D). The frequencies of BM LT-HSCs and MPPs were higher in *Vav*$^{Cre+}$*Rxrab*$^{fl/fl}$ mice on posttreatment day 20 (Figure 4E), and BrdU labeling revealed higher proliferation rates of *Vav*$^{Cre+}$*Rxrab*$^{fl/fl}$ LSKs and LT-HSCs on post–5-FU treatment day 5 (Figure 4F-G). These results indicate that RXRα;RXRβ expression is required for the maintenance of HSC quiescence and death rate in steady-state and stress hematopoiesis.

RXRα;RXRβ-deficient HSCs have an aged-like gene signature and show MYC signaling pathway activation and alternative splicing with intron retention

We performed a bulk RNA-seq analysis on LT-HSCs and MPPs from 5-month-old WT and *Vav*$^{Cre+}$*Rxrab*$^{fl/fl}$ mice. Analysis of the predominant gene expression patterns identified uniquely expressed transcripts in each of the separate gates (Figure 5A). Although gene expression differed between *Vav*$^{Cre+}$*Rxrab*$^{fl/fl}$ LT-HSCs and MPPs and their WT counterparts, the greatest between-sample differences were by cell state rather than genotype. This observation was further supported by principal component (PC) analysis of detectable genes, which showed that the major source of variance (PC1, 47%) was cell state, with PC2 corresponding to genotype (Figure 5B). *Vav*$^{Cre+}$*Rxrab*$^{fl/fl}$ LT-HSCs were characterized by predominant upregulation of gene expression (fold change [FC] ≥ 1.5 or ≤ −1.5; adjusted $P \leq 0.1$) (Figure 5C; supplemental

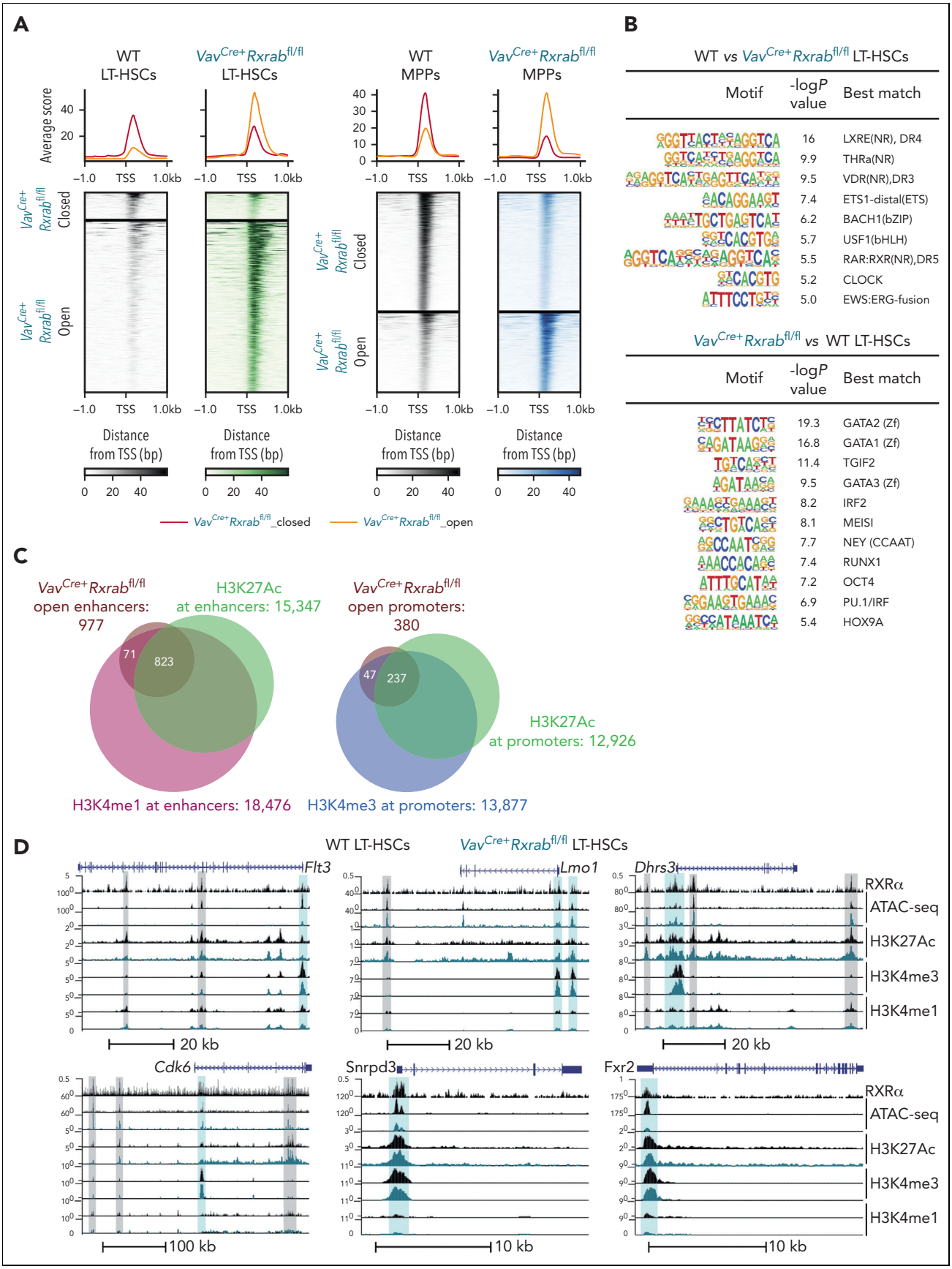
A
WT LT-HSCs
Vav^Cre+ Rxrab^fl/fl LT-HSCs
WT MPPs
Vav^Cre+ Rxrab^fl/fl MPPs
Average score
Vav^Cre+ Rxrab^fl/fl Closed
Vav^Cre+ Rxrab^fl/fl Open
−1.0 TSS 1.0kb
Distance from TSS (bp)
0 20 40
Vav^Cre+ Rxrab^fl/fl_closed
Vav^Cre+ Rxrab^fl/fl_open
B
WT vs Vav^Cre+ Rxrab^fl/fl LT-HSCs
Motif
-logP value
Best match
16 LXRE(NR), DR4
9.9 THRa(NR)
9.5 VDR(NR),DR3
7.4 ETS1-distal(ETS)
6.2 BACH1(bZIP)
5.7 USF1(bHLH)
5.5 RAR:RXR(NR),DR5
5.2 CLOCK
5.0 EWS:ERG-fusion
Vav^Cre+ Rxrab^fl/fl vs WT LT-HSCs
Motif
-logP value
Best match
19.3 GATA2 (Zf)
16.8 GATA1 (Zf)
11.4 TGIF2
9.5 GATA3 (Zf)
8.2 IRF2
8.1 MEISI
7.7 NEY (CCAAT)
7.4 RUNX1
7.2 OCT4
6.9 PU.1/IRF
5.4 HOX9A
C
Vav^Cre+ Rxrab^fl/fl open enhancers: 977
H3K27Ac at enhancers: 15,347
71
823
Vav^Cre+ Rxrab^fl/fl open promoters: 380
47
237
H3K27Ac at promoters: 12,926
H3K4me1 at enhancers: 18,476
H3K4me3 at promoters: 13,877
D
WT LT-HSCs
Vav^Cre+ Rxrab^fl/fl LT-HSCs
Flt3
Lmo1
Dhrs3
Cdk6
Snrpd3
Fxr2
RXRα
ATAC-seq
H3K27Ac
H3K4me3
H3K4me1
20 kb
100 kb
10 kb

Figure 6.

Tables 2 and 3). In contrast, $Vav^{Cre+}Rxrab^{fl/fl}$ MPPs showed prominent transcript downregulation vs WT MPPs (FC ≥ 1.5 or ≤ −1.5; adjusted $P \leq 0.1$) (supplemental Figure 8A; supplemental Tables 4 and 5). Top downregulated genes in $Vav^{Cre+}Rxrab^{fl/fl}$ LT-HSCs included molecules important for lymphoid and erythroid development and function (*Klf9* and *Sptb*)[40,41] and *Pdk4*, which is essential for LT-HSC cell-cycle quiescence and metabolism[42] (Figure 5C; supplemental Tables 2 and 3).

Gene ontology enrichment analysis revealed that downregulated pathways in $Vav^{Cre+}Rxrab^{fl/fl}$ LT-HSCs were associated with splicing regulation and erythrocyte development, whereas enriched pathways included cell-cell adhesion and leukocyte function (supplemental Figure 8B-C). In $Vav^{Cre+}Rxrab^{fl/fl}$ MPPs, upregulated pathways were related to oxidative stress, whereas downregulated pathways included tumor necrosis factor-α and interleukin-6 production and T-cell activation (supplemental Figure 8B-C). Differentially expressed genes (DEGs) in $Vav^{Cre+}Rxrab^{fl/fl}$ LT-HSCs included genes previously reported to be deregulated in aged HSCs[43] (Figure 5D). Other DEGs in $Vav^{Cre+}Rxrab^{fl/fl}$ LT-HSCs included MYC targets[44] and RNA processing and splicing regulators (Figure 5D). To determine whether RNA splicing alterations might be involved in the aged-HSC signature of $Vav^{Cre+}Rxrab^{fl/fl}$ LT-HSCs, we evaluated alternative splicing and intron retention.[31,45,46] This analysis identified 1841 unique known and novel alternative splicing events differentiating WT from $Vav^{Cre+}Rxrab^{fl/fl}$ LT-HSCs, and 1638 events differentiating WT from $Vav^{Cre+}Rxrab^{fl/fl}$ MPPs (empirical Bayes moderated *t*-test $P < .05$) (Figure 5E). By considering inclusion (exon/intron gain) and exclusion (exon/intron loss) separately, we found that most events involved differential intron retention, preferentially in $Vav^{Cre+}Rxrab^{fl/fl}$ LT-HSCs (Figure 5E). Alternative splicing specific to $Vav^{Cre+}Rxrab^{fl/fl}$ LT-HSCs was associated with programmed cell death (eg, *Madd*), cell-cycle arrest (eg, *Araf*), chromatin modification (eg, *Araf*), NR-mediated signaling (eg, *Carm1*), thiol-ester hydrolase activity (eg, *Usp20*), and cell-cell communication (eg, *Itga5*); these findings were verified by genomic read visualization (Figure 5F). Significantly regulated splicing inclusion events in $Vav^{Cre+}Rxrab^{fl/fl}$ LT-HSCs were enriched in genes linked to GTPase activity and cell death, whereas significantly regulated exclusion splicing events were enriched in genes involved in the cell cycle, autophagy, and stress response control (Gene Ontology) (supplemental Figure 8D).

To generate a genome-wide profile of RXR binding in LT-HSCs and MPPs, we performed RXRα CUT&RUNseq assays. This analysis identified >6352 binding sites in LT-HSCs and >21 046 RXR binding sites in MPPs, with sites preferentially located in promoter and upstream regions (Figure 5G; supplemental Figure 8E; supplemental Tables 6 and 7). Overlap analysis with bulk RNA-seq data demonstrated that a high number of DEGs in $Vav^{Cre+}Rxrab^{fl/fl}$ cells were directly regulated by RXRs (Figure 5H; supplemental Figure 8F). Motif analysis of LT-HSC RXR peaks indicated enrichment for RXR binding sites and for TFs essential for the maintenance and differentiation of HSCs, including erythroblast transformation specific (ETS) translocation variant 4 (ETV4),[47] specificity protein 1 (SP1),[48] and cyclic AMP-dependent transcription factor (ATF3)[49] (Figure 5I). Similar data were obtained in MPPs (supplemental Figure 8G). Functional annotation clustering analysis of the RXR cistrome identified a variety of enriched pathways in LT-HSCs and MPPs, including cell cycle and the MYC pathway, as well as processes involved in mRNA processing and splicing (Figure 5J; supplemental Figure 8H). Our results provide evidence that RXRs function as master TFs that maintain a young-like HSC transcriptional signature, low MYC-dependent transcriptional activity, and appropriate splicing in LT-HSCs.

RXR deficiency leads to chromatin openness at promoter and enhancer regions in LT-HSCs

Assay for transposase-accessible chromatin with sequencing (ATAC-seq) revealed a strong spike in chromatin-accessible peaks in $Vav^{Cre+}Rxrab^{fl/fl}$ vs WT LT-HSCs (z score ≤ −2 or ≥ 2; $P \leq .05$) (Figure 6A; supplemental Tables 8 and 9), indicating that RXRα;RXRβ deficiency leads to chromatin openness in LT-HSCs. In contrast, $Vav^{Cre+}Rxrab^{fl/fl}$ MPPs had a higher proportion of closed peaks than WT MPPs (FC ≤ −2 or ≥ 2; false discovery rate ≤ 0.05) (Figure 6A; supplemental Tables 10 and 11). Analysis of peak distribution demonstrated a reorganization of the chromatin landscape in $Vav^{Cre+}Rxrab^{fl/fl}$ LT-HSCs but not MPPs (supplemental Figure 9A-B). Motif enrichment analysis showed a reduction in peaks enriched in binding sites for NRs in $Vav^{Cre+}Rxrab^{fl/fl}$ LT-HSCs and MPPs ($P \leq .01$; Figure 6B; supplemental Figure 9C). Conversely, $Vav^{Cre+}Rxrab^{fl/fl}$ LT-HSCs were highly enriched in binding sites for several TFs with roles in hematopoiesis, including the master hematopoiesis regulators GATA (consensus DNA sequence [T/A]GATA[A/G])-binding factors GATA1, GATA2, and GATA3[50] and RUNT-related transcription factor 1 (RUNX1)[51]; myeloid ecotropic viral integration site 1 (MEIS1), which is overexpressed in certain leukemias[52]; the myeloid differentiation master TF PU.1[53]; and the HSC-activity marker homeobox protein Hox-A9 (HOX9A)[54] (Figure 6B). Similar binding-site enrichment was found in $Vav^{Cre+}Rxrab^{fl/fl}$ MPPs (supplemental Figure 9C). Overlap analysis between RXR-binding sites and $Vav^{Cre+}Rxrab^{fl/fl}$ vs WT differentially accessible regions (DARs) revealed that around 50% of changes in MPP chromatin accessibility were RXR dependent, whereas a lower proportion of DARs colocalized with RXR-binding sites in LT-HSCs (supplemental Figure 9D-E).

We performed CUT&RUNseq assays to determine the monomethylation and trimethylation status of lysine 4 (H3K4me1 and

Figure 6. Chromatin openness at enhancer and promoter sites in RXRα;RXRβ-deficient LT-HSCs. (A) Heat map of assay for transposase-accessible chromatin with sequencing (ATAC-seq) signals located in transcription start site (TSS) flanking regions (±1 kb) in 5-month-old $Vav^{Cre+}Rxrab^{fl/fl}$ and WT LT-HSCs and MPPs. (B) HOMER known motif analysis of ATAC-seq peaks. The top panels shows transcription factor motifs enriched in WT LT-HSCs relative to the background of $Vav^{Cre+}Rxrab^{fl/fl}$ LT-HSC peaks. The bottom panel shows transcription factor motifs enriched in $Vav^{Cre+}Rxrab^{fl/fl}$ LT-HSCs relative to the background of WT LT-HSC peaks. (C) Peak annotations identified in an overlap analysis between the open promoter and enhancer regions in LT-HSCs identified in the ATAC-seq experiment (defined by genomic distribution; see also supplemental Figure 8A), and regions marked by high H3K4me3 and H3K27Ac, and ±1 kb from TSS (putative promoters), high H3K4me1 and H3K27Ac, and >1 kb and <−1 kb from the TSS (putative active enhancers), and high H3K4me1 but no H3K27Ac, and >1 kb and <−1 kb from the TSS (putative poised enhancers). (D) University of California, Santa Cruz (UCSC) genome browser track examples of active enhancers (vertical gray highlights) and promoters (vertical blue highlights) within *loci* that overlap RXRα CUT&RUNseq and ATAC-seq peaks.

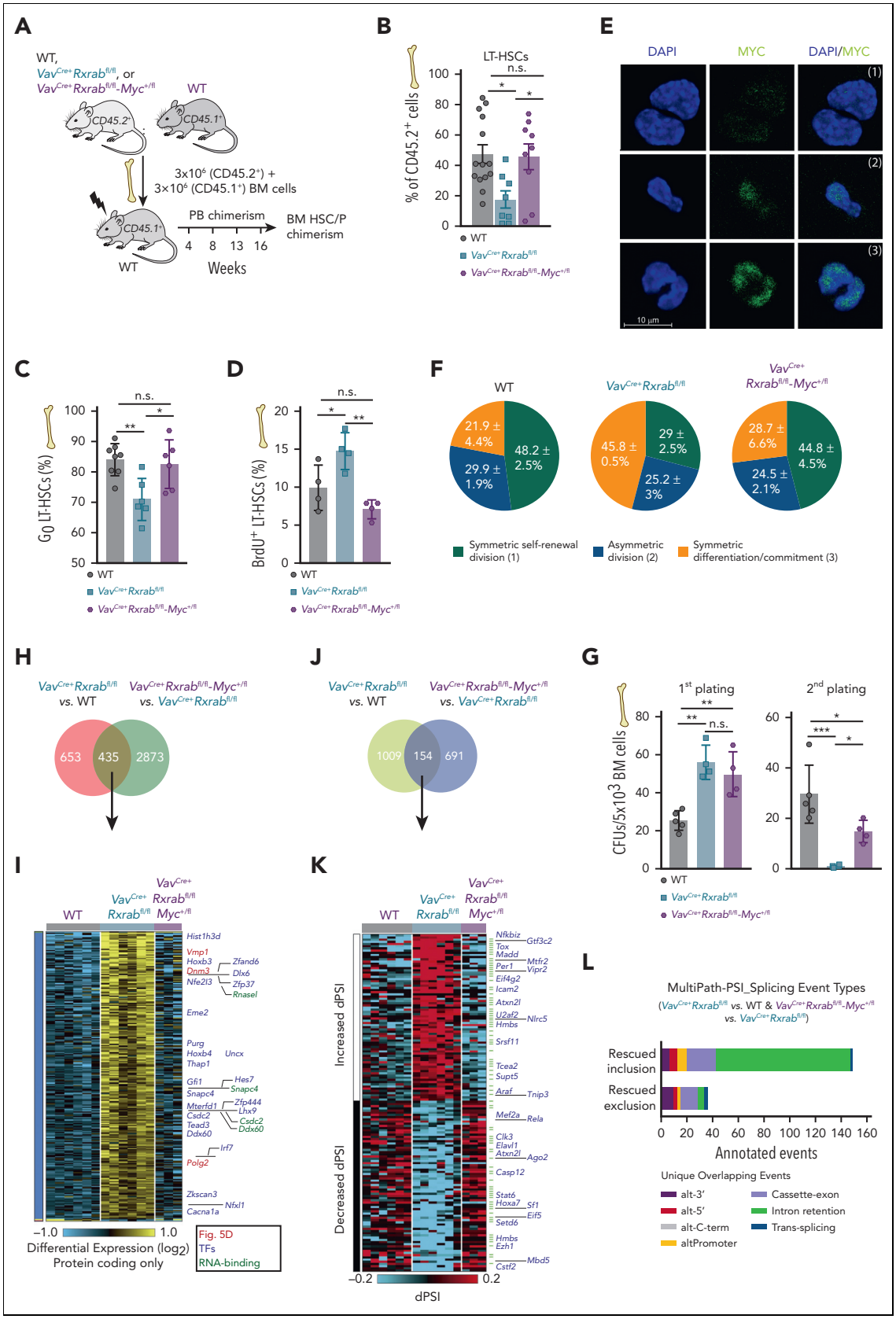

Figure 7. *Myc* haploinsufficiency rescues regeneration, transcriptome, and spliceosome of phenotypically identifiable LT-HSCs. (A-B) Competitive transplantation assay of unfractionated BM cells from 4-month-old WT, *Vav*$^{Cre+}$*Rxrab*$^{fl/fl}$, and *Vav*$^{Cre+}$*Rxrab*$^{fl/fl}$-*Myc*$^{+/fl}$ mice (CD45.2$^+$) in a 1:1 ratio with C57BL/6 BM cells (CD45.1$^+$) into lethally irradiated C57BL/6 mice (CD45.1$^+$) (data pooled from 2 independent experiments). (A) Experimental scheme. (B) Percentages of CD45.2$^+$ BM LT-HSCs at 16 weeks after transplantation. (C) Frequencies of CD150$^+$CD48$^-$ LT-HSCs from WT, *Vav*$^{Cre+}$*Rxrab*$^{fl/fl}$, and *Vav*$^{Cre+}$*Rxrab*$^{fl/fl}$-*Myc*$^{+/fl}$ mice in the G_0 phase of the cell cycle (pyronin

H3K4me3) and the acetylation status of lysine 27 (H3K27ac) in histone 3 (supplemental Figure 9F). An overlap analysis between open DARs and regions marked by (1) high H3K4me3 and H3K27Ac (located ±1 kb from a transcription start site [TSS]; putative promoters), (2) high H3K4me1 and H3K27Ac (located >1 kb and <−1 kb from a TSS; putative active enhancers), and (3) high H3K4me1 but no H3K27Ac (located >1 kb and <−1 kb from a TSS; putative poised enhancers) revealed that most open DARs in $Vav^{Cre+}Rxrab^{fl/fl}$ LT-HSCs coincided with active promoters and enhancers (Figure 6C). Double H3K4me3;H3K27Ac- and/or H3K4me1;H3K27Ac-enriched regions overlapping with RXR-binding sites and DARs were found in *loci* harboring HSC-aging signature genes,[43] leukemia oncogenes, MYC targets, and RNA processing genes, including *Flt3*, *Lmo1*, *Dhrs3*, *Cdk6*, *Snrpd3*, and *Fxr2* (Figure 6D). These data indicate that RXRs contribute to the LT-HSC maintenance of chromatin condensation and transcriptional repression, which are hallmarks of cell quiescence.[55]

Myc haploinsufficiency rescues regeneration of phenotypically identifiable LT-HSCs in RXR-deficient mice

To determine if MYC mediates the role of RXRs in HSC fitness, we crossed *Myc*-haploinsufficient mice[56] with $Vav^{Cre+}Rxrab^{fl/fl}$ mice, generating $Vav^{Cre+}Rxrab^{fl/fl}$-$Myc^{+/fl}$ mice. The functional capacities of equal numbers of BM HSC/Ps from WT, $Vav^{Cre+}Rxrab^{fl/fl}$, or $Vav^{Cre+}Rxrab^{fl/fl}$-$Myc^{+/fl}$ mice were tested in competitive repopulation assays (Figure 7A; supplemental Figure 10A). Although the PB donor contribution of $Vav^{Cre+}Rxrab^{fl/fl}$-$Myc^{+/fl}$ mice was even lower than that of $Vav^{Cre+}Rxrab^{fl/fl}$ mice (supplemental Figure 10B), *Myc* haploinsufficiency rescued the regeneration of LT-HSCs (but not other HSC/Ps) (Figure 7B; supplemental Figure 10C). Cell-cycle analysis showed that *Myc* haploinsufficiency restored the level of $Vav^{Cre+}Rxrab^{fl/fl}$ LT-HSCs in G_0 phase and the percentage of proliferating cells back to WT levels (Figure 7C-D). We performed a pair-daughter first HSC division assay, in which MYC upregulation in daughter cells is a hallmark of loss of self-renewing divisions.[57,58] Lack of RXRs entailed an approximately twofold increase in the frequency of differentiated/committed daughter cells, concomitant with a reduction in symmetric self-renewal division modes (Figure 7E-F). These changes in fate division were restored to WT levels in $Vav^{Cre+}Rxrab^{fl/fl}$-$Myc^{+/fl}$ mice (Figure 7E-F). The rescue of self-renewing cells was also observed in vitro by serial plating analysis (Figure 7G). However, *Myc* haploinsufficiency did not restore the pre–B-cell progenitor content in BM (supplemental Figure 10D).

Next, we performed bulk RNA-seq in WT, $Vav^{Cre+}Rxrab^{fl/fl}$, and $Vav^{Cre+}Rxrab^{fl/fl}$-$Myc^{+/fl}$ LT-HSCs. Analyses of these data show that *Myc* haploinsufficiency partially restores $Vav^{Cre+}Rxrab^{fl/fl}$ transcriptional (40%) and splicing (13%) defects (Figure 7H-L; supplemental Figure 10E; supplemental Tables 12-15). Rescued DEGs included diverse transcriptional regulators (eg, *Gfi1* and *Irf7*) and few RNA-binding proteins (eg, *RnaseI* and *Snapc4*) (Figure 7I). Although only a small percentage of RXR-dependent splicing events were rescued (Figure 7J-L), 62% of them were enriched in the reversal of intron retention in genes involved in posttranscriptional regulation (eg, *Sf1* and *U2af2*), regulation of translation (eg, *Tcea2* and *Ago2*), chromatin DNA binding (eg, *Tox* and *Per1*), and transcriptional regulation (eg, *Sp100* and *Setd6*) (Figure 7K). Our results demonstrate that MYC activity is the key RXR-dependent molecular regulator of LT-HSC fitness, in vivo regeneration activity, as well as transcriptome and spliceosome.

Discussion

In this study, we demonstrate that RXRs are essential for the maintenance of HSC activity and balanced hematopoietic differentiation. Dual lack of RXRα and RXRβ in HSCs leads to chromatin openness and the acquisition of a premature aged-like transcriptional and phenotypic signature in LT-HSCs. As a result, these cells transition from a dormant to a proliferative and transcriptionally active state characterized by MYC activity upregulation and intron retention, which lead to the exhaustion of functional HSCs. This manifests in lymphopenia and a myeloid/megakaryocyte-skewed hematopoietic system in RXRα;RXRβ-deficient mice that eventually progresses to fatal MPD in the context of myeloproliferation-associated inflammation and hemostatic defects similar to those observed in other mouse models of fatal MPD.[26,59]

Chromatin openness and transcriptional activation of RXRα;RXRβ-deficient HSCs contrasts the transcriptional downregulation and reduced chromatin accessibility of RXRα;RXRβ-deficient committed cells, suggesting that the mechanisms driving RXR control over HSC quiescence and lineage choice are cell context dependent. The complexity of mechanisms that can be controlled by RXRs might be explained by their

Figure 7 (continued) Y^-/Hoechst 33342$^-$; data pooled from 3 independent experiments). (D) Percentage of 5-bromo-2′-deoxyuridine–positive ($BrdU^+$) $CD150^+CD48^-$ LT-HSCs from WT, $Vav^{Cre+}Rxrab^{fl/fl}$, and $Vav^{Cre+}Rxrab^{fl/fl}$-$Myc^{+/fl}$ mice after 1-hour pulse with BrdU. (E-F) Immunofluorescence analysis, showing different division modes according to MYC expression in paired daughter LT-HSCs from WT, $Vav^{Cre+}Rxrab^{fl/fl}$, and $Vav^{Cre+}Rxrab^{fl/fl}$-$Myc^{+/fl}$ mice. (E) Representative images showing (1) symmetric self-renewal (absence of MYC expression in paired daughter cells), (2) asymmetric division (high vs low MYC expression in paired daughter cells), and (3) symmetric differentiation/commitment (MYC expression in both cells); scale bar, 10 μm. (F) Percentage of LT-HSCs corresponding to division modes 1, 2, and 3 as in E; n = 60 division pairs captured from 5 WT mice; n = 48 division pairs captured from 3 $Vav^{Cre+}Rxrab^{fl/fl}$ mice; and n = 37 division pairs captured from 5 $Vav^{Cre+}Rxrab^{fl/fl}$-$Myc^{+/fl}$ mice. Analyses were performed in 2 independent experiments. (G) Serial CFU plating assay in total BM cells from WT, $Vav^{Cre+}Rxrab^{fl/fl}$, or $Vav^{Cre+}Rxrab^{fl/fl}$-$Myc^{+/fl}$ mice. (H-L) Bulk transcriptome of WT, $Vav^{Cre+}Rxrab^{fl/fl}$, and $Vav^{Cre+}Rxrab^{fl/fl}$-$Myc^{+/fl}$ LT-HSCs. Normalized expression values from bulk RNA-seq data are provided in supplemental Tables 12-15. (H) Rescued differentially expressed genes in $Vav^{Cre+}Rxrab^{fl/fl}$-$Myc^{+/fl}$ vs $Vav^{Cre+}Rxrab^{fl/fl}$ LT-HSCs (eBayes *t*-test $P < .05$; fold > 1.2), compared with $Vav^{Cre+}Rxrab^{fl/fl}$-$Myc^{+/fl}$ vs WT LT-HSCs (eBayes *t*-test $P < .05$; false discovery rate corrected; fold > 1.5). (I) Heat map of the 435 rescued genes showing silencing of $Vav^{Cre+}Rxrab^{fl/fl}$ LT-HSC–induced transcripts by $Myc^{+/fl}$ expression. On the left are shown example rescued genes (Figure 5D; TFs or RNA-binding regulators). (J) Rescued alternative splicing events in $Vav^{Cre+}Rxrab^{fl/fl}$-$Myc^{+/fl}$ vs $Vav^{Cre+}Rxrab^{fl/fl}$ LT-HSCs, compared with $Vav^{Cre+}Rxrab^{fl/fl}$-$Myc^{+/fl}$ vs WT LT-HSCs (eBayes *t*-test $P < .05$; δ percentage spliced in [PSI] > 0.1 for both comparisons). (K) Heat map of 154 unique splicing events, organized by increased junction PSI value in $Vav^{Cre+}Rxrab^{fl/fl}$ vs WT LT-HSCs, with exemplar intron retention events (green tick mark) and genes symbols called out. (L) Number of observed unique annotated splicing events in the 154 rescued splicing events, by exon/intron inclusion or exclusion. Splicing events associated with exon or intron inclusion (increased relative expression) vs exclusion are shown separately. Results are presented as means ± SEM, and dots represent individual animals. Significance was determined by ordinary 1-way analysis of variance, and is represented as follows: $*P \le .05$, $**P \le .01$, and $***P \le .001$. DAPI, 4′,6-diamidino-2-phenylindole; n.s., not significant.

promiscuity; RXRs regulate several NRs via direct dimerization and binding of cognate ligands and coactivators, as demonstrated in other cell types (reviewed by De Bosscher et al[60]). Our TF motif analysis indicates that RXR/RAR binding sites are overrepresented in the LT-HSC signature, pointing to RXR/RAR signaling as an important player in RXR-mediated control of HSC fitness.[5] Accordingly, recent studies demonstrated that vitamin A signaling, and especially nonclassic retinoid signaling mediated by cytochrome P450 family 26 subfamily B member (CYP26B1) and 4-oxo-RA, regulates the dormancy and LT repopulation capacity of mouse HSCs through RXR/RARβ.[14] The cell-autonomous mechanism of this regulatory path may be species specific, because *Cyp29b1* is expressed in mouse HSCs, whereas in humans it is expressed in BM niche but not HSC cells.[13,14] Our study supports a role for RXRs in mouse HSC fitness beyond their collaborative role in RXR/RARβ heterodimers. Considering that RXRs play an active role in response to retinoids,[61] remaining transcriptional effects in *Rarb*-knockout HSCs treated with retinoids[14] might be explained by RARβ-independent RXR activation. In addition, although both *Rarb*- and *Cyp26b1*-deficient mice present diminished HSC self-renewal capacities,[14] none of these mice recapitulates the profound phenotype of RXRα;RXRβ-deficient mice. For example, unlike RXRα;RXRβ-deficient LT-HSCs, HSC lacking nonclassic retinoid signaling retain radioprotection ability. This suggests that signaling pathways other than retinoids contribute to the role of RXRs in the control of LT-HSC fitness. Several recent research lines point to FAs as RXR ligands that provide a metabolic link to HSC biology. FA metabolism is specifically enriched in LT-HSCs relative to progenitor cells.[14] More important, we identified the long-chain FA C24:5 as a natural ligand of RXRs in HSCs, both under basal and stressed hematopoiesis.[62] Moreover, FA metabolism is upregulated in HSCs from old mice,[63] and HSC functionality is recovered after treatment with y-linoleic acid in both aged humans and mice.[63] Thus, although RA seems to have different effects in humans and mice,[13,64] HSC responses to FA treatment are similar in both species. Future studies could explore whether combination of a retinoid with FAs could improve ex vivo expansion of human HSCs and offer a route toward stem-cell gene therapy.

Another important finding is that the loss of one *Myc* allele prevented the loss of quiescence and self-renewal, in vivo regeneration capacity, and the changes in the transcriptional and splicing regulatory landscapes of RXRα;RXRβ-deficient HSCs. Our results demonstrate that MYC activity lies at the root of the HSC phenotype associated with loss of RXR signaling. Interestingly, a normal distribution of progeny downstream of LT-HSCs was not restored, suggesting that MYC is indispensable for the initial phase of LT-HSC fate commitment but not for differentiation in later divisions. This is in agreement with previous studies demonstrating that MYC expression is low in dormant HSCs but increases during the transition toward active HSCs and subsequently multipotent progenitors.[5] Beyond the known role of MYC in the control of self-renewal,[65] our results suggest that MYC signaling activation in RXRα;RXRβ-deficient HSCs promotes a phenotype compatible with HSC aging through the control of alternative splicing, leading to global intron retention.[66,67] The mechanisms by which MYC performs this transcriptional activity might be direct or indirect. MYC activation has the potential to impact HSC fitness, because alterations to ribosomal biogenesis and RNA splicing contribute to age-associated HSC epigenetic reprogramming[68] and to myelodysplastic-related disorders and leukemia.[69,70] Our results demonstrate that lack of RXRα;RXRβ in HSCs triggers a spike in intron retention in LT-HSCs, with extensive alteration to genes and processes involved in mRNA processing and splicing, through a MYC-dependent mechanism. Despite intense biological research over several decades, pharmacologic inhibition of MYC remains ineffective because of its "undruggable" protein structure.[71] Our study points to RXRs as potential druggable targets for maintaining HSC fitness during transplantation procedures and protecting against premature HSC aging and MPD.

Acknowledgments

The authors thank the members of the J.A.C. and M.R. laboratories for extensive discussions and critiques of the manuscript. The authors thank Daniel Metzger (Université de Strasbourg, Strasbourg, France) for *Rxrb*$^{f/f}$ mice, Juan Carlos Zúñiga-Pflücker (Sunnybrook Health Sciences Centre, Toronto, ON, Canada) for OP9NL1 cells, Daniel Jiménez-Carretero (Centro Nacional de Investigaciones Cardiovasculares [CNIC]) for t-distributed stochastic neighbor embedding (t-SNE) analysis, the Centre for Genomic Regulation (CRG; Barcelona, Spain) Genomics Unit for assay for transposase-accessible chromatin with sequencing, and S. Bartlett (CNIC) for editorial assistance. The authors also thank the staff of the CNIC Cellomics and Animal facilities for technical support.

This study was supported by grants from the Spanish Ministerio de Ciencia e Innovación (MICIN) (SAF2017-90604-REDT-NurCaMein, RTI2018-095928-B100, and PID2021-122552OB-I00), La Marató de TV3 Foundation (201605-32), and the Comunidad de Madrid (MOIR-B2017/BMD-3684) (M.R.) and from the Formación de Profesorado Universitario (FPU17/01731) program (MICIN) (J.P.). The project also received funding from the US National Institutes of Health (R01 DK124115, P01 HL158688, R01 HL147536, R01 CA237016, and U54 DK126108) (J.A.C.). The Centro Nacional de Investigaciones Cardiovasculares (CNIC) is supported by the Instituto de Salud Carlos III, the Ministerio de Ciencia e Innovación, and the Pro CNIC Foundation and is a Severo Ochoa Center of Excellence (grant CEX2020-001041-S funded by Spanish Ministerio de Ciencia e Innovación/Agencia Estatal de Investigación [MICIN/AEI/10.13039/501100011033]).

Authorship

Contribution: M.P.M.-G., J.P., J.S.W., J.A.C., and M.R. conceptualized the study; M.P.M.-G., J.P., R.N., A. Paredes, H.N., and V.N. performed methods; R.N., M.J.G., A. Paranjpe, A.B., D.J.S., F.S.-C., and N.S. performed software analysis; M.P.M.-G., J.P., R.N., A. Paranjpe, H.N., and M.J.G. performed data interpretation and analysis; M.P.M.-G., J.P., J.S.W., N.S., J.A.C., and M.R. wrote, reviewed, and edited the manuscript; J.A.C. and M.R. supervised the project; and J.A.C. and M.R. obtained funding.

Conflict-of-interest disclosure: The authors declare no competing financial interests.

ORCID profiles: M.P.M.-G., 0000-0001-8045-2995; J.P., 0000-0002-7423-9706; A. Paredes, 0000-0003-3119-8788; M.J.G., 0000-0002-4111-4835; A.B., 0000-0002-4459-4926; F.S.-C., 0000-0003-1881-1664; J.S.W., 0000-0001-6656-3672; N.S., 0000-0001-9689-2469; J.A.C., 0000-0002-1291-7233; M.R., 0000-0002-8090-8902.

Correspondence: Mercedes Ricote, Centro Nacional de Investigaciones Cardiovasculares (CNIC), Melchor Fernández Almagro, 3, 28029 Madrid, Spain; email: mricote@cnic.es; and Jose A. Cancelas, Hoxworth Blood Center, 3130 Highland Ave, Cincinnati, OH 45267; email: jose.cancelas@cchmc.org.

Footnotes

Submitted 28 April 2022; accepted 30 October 2022; prepublished online on *Blood* First Edition 8 November 2022. https://doi.org/10.1182/blood.2022016832.

*M.P.M.-G. and J.P. contributed equally to this study.

Transcriptomic data are deposited in the National Center for Biotechnology Information's Gene Expression Omnibus, with accession numbers GSE191163 and GSE199937.

The online version of this article contains a data supplement.

The publication costs of this article were defrayed in part by page charge payment. Therefore, and solely to indicate this fact, this article is hereby marked "advertisement" in accordance with 18 USC section 1734.

REFERENCES

1. Cabezas-Wallscheid N, Klimmeck D, Hansson J, et al. Identification of regulatory networks in HSCs and their immediate progeny via integrated proteome, transcriptome, and DNA methylome analysis. *Cell Stem Cell*. 2014;15(4):507-522.
2. Kruta M, Sunshine MJ, Chua BA, et al. Hsf1 promotes hematopoietic stem cell fitness and proteostasis in response to ex vivo culture stress and aging. *Cell Stem Cell*. 2021;28(11):1950-1965.e1956.
3. Akunuru S, Geiger H. Aging, clonality, and rejuvenation of hematopoietic stem cells. *Trends Mol Med*. 2016;22(8):701-712.
4. Zhang Y, Wong J, Klinger M, Tran MT, Shannon KM, Killeen N. MLL5 contributes to hematopoietic stem cell fitness and homeostasis. *Blood*. 2009;113(7):1455-1463.
5. Cabezas-Wallscheid N, Buettner F, Sommerkamp P, et al. Vitamin A-retinoic acid signaling regulates hematopoietic stem cell dormancy. *Cell*. 2017;169(5):807-823.e819.
6. Rőszer T, Menendez-Gutierrez MP, Cedenilla M, Ricote M. Retinoid X receptors in macrophage biology. *Trends Endocrinol Metab*. 2013;24(9):460-468.
7. Krezel W, Ruhl R, de Lera AR. Alternative retinoid X receptor (RXR) ligands. *Mol Cell Endocrinol*. 2019;491:110436-110454.
8. Gratas C, Menot M-L, Dresch D, Chomienne C. Retinoic acid supports granulocytic but not erythrocytic differentiation of myeloid progenitors in normal bone marrow. *Leukemia*. 1993;7(8):1156-1162.
9. Labrecque J, Allan D, Chambon P, Iscove NN, Lohnes D, Hoang T. Impaired granulocytic differentiation in vitro in hematopoietic cells lacking retinoic acid receptors alpha1 and gamma. *Blood*. 1998;92(2):607-615.
10. Purton LE, Bernstein ID, Collins SJ. All-trans retinoic acid delays the differentiation of primitive hematopoietic precursors (lin-c-kit+Sca-1(+)) while enhancing the terminal maturation of committed granulocyte/monocyte progenitors. *Blood*. 1999;94(2):483-495.
11. Chute JP, Muramoto GG, Whitesides J, et al. Inhibition of aldehyde dehydrogenase and retinoid signaling induces the expansion of human hematopoietic stem cells. *Proc Natl Acad Sci U S A*. 2006;103(31):11707-11712.
12. Purton LE, Bernstein ID, Collins SJ. All-trans retinoic acid enhances the long-term repopulating activity of cultured hematopoietic stem cells. *Blood*. 2000;95(2):470-477.
13. Ghiaur G, Yegnasubramanian S, Perkins B, Gucwa JL, Gerber JM, Jones RJ. Regulation of human hematopoietic stem cell self-renewal by the microenvironment's control of retinoic acid signaling. *Proc Natl Acad Sci U S A*. 2013;110(40):16121-16126.
14. Schonberger K, Obier N, Romero-Mulero MC, et al. Multilayer omics analysis reveals a non-classical retinoic acid signaling axis that regulates hematopoietic stem cell identity. *Cell Stem Cell*. 2022;29(1):131-148.e10.
15. Safi R, Muramoto GG, Salter AB, et al. Pharmacological manipulation of the RAR/RXR signaling pathway maintains the repopulating capacity of hematopoietic stem cells in culture. *Mol Endocrinol*. 2009;23(2):188-201.
16. Sakashita A, Kizaki M, Pakkala S, et al. 9-Cis-retinoic acid: effects on normal and leukemic hematopoiesis in vitro. *Blood*. 1993;81(4):1009-1016.
17. Ricote M, Snyder CS, Leung HY, Chen J, Chien KR, Glass CK. Normal hematopoiesis after conditional targeting of RXRalpha in murine hematopoietic stem/progenitor cells. *J Leukoc Biol*. 2006;80(4):850-861.
18. Delgado MD, Leon J. Myc roles in hematopoiesis and leukemia. *Genes Cancer*. 2010;1(6):605-616.
19. Salomonis N. Investigating cell fate decisions with ICGS analysis of single cells. *Methods Mol Biol*. 2019;1975:251-275.
20. Buenrostro JD, Wu B, Chang HY, Greenleaf WJ. ATAC-seq: a method for assaying chromatin accessibility genome-wide. *Curr Protoc Mol Biol*. 2015;109(suppl 109):21.29.1-21.29.9.
21. Skene PJ, Henikoff JG, Henikoff S. Targeted in situ genome-wide profiling with high efficiency for low cell numbers. *Nat Protoc*. 2018;13(5):1006-1019.
22. Pietras EM, Reynaud D, Kang YA, et al. Functionally distinct subsets of lineage-biased multipotent progenitors control blood production in normal and regenerative conditions. *Cell Stem Cell*. 2015;17(1):35-46.
23. Kühn R, Schwenk F, Aguet M, Rajewsky K. Inducible gene targeting in mice. *Science*. 1995;269(5229):1427-1429.
24. de Boer J, Williams A, Skavdis G, et al. Transgenic mice with hematopoietic and lymphoid specific expression of Cre. *Eur J Immunol*. 2003;33(2):314-325.
25. Kogan SC, Ward JM, Anver MR, et al. Bethesda proposals for classification of nonlymphoid hematopoietic neoplasms in mice. *Blood*. 2002;100(1):238-245.
26. Thomas EK, Cancelas JA, Chae HD, et al. Rac guanosine triphosphatases represent integrating molecular therapeutic targets for BCR-ABL-induced myeloproliferative disease. *Cancer Cell*. 2007;12(5):467-478.
27. Rodriguez-Fraticelli AE, Weinreb C, Wang SW, et al. Single-cell lineage tracing unveils a role for TCF15 in haematopoiesis. *Nature*. 2020;583(7817):585-589.
28. Carrelha J, Meng Y, Kettyle LM, et al. Hierarchically related lineage-restricted fates of multipotent haematopoietic stem cells. *Nature*. 2018;554(7690):106-111.
29. Regan-Komito D, Swann JW, Demetriou P, et al. GM-CSF drives dysregulated hematopoietic stem cell activity and pathogenic extramedullary myelopoiesis in experimental spondyloarthritis. *Nat Commun*. 2020;11(1):155-170.
30. Zhang YH, Hu Y, Zhang Y, Hu LD, Kong X. Distinguishing three subtypes of hematopoietic cells based on gene expression profiles using a support vector machine. *Biochim Biophys Acta Mol Basis Dis*. 2018;1864(6 pt B):2255-2265.
31. Muench DE, Ferchen K, Velu CS, et al. SKI controls MDS-associated chronic TGF-beta signaling, aberrant splicing, and stem cell fitness. *Blood*. 2018;132(21):e24-e34.
32. Zhang J, Yang P, Liu D, et al. c-Myc upregulated by high glucose inhibits HaCaT differentiation by S100A6 transcriptional activation. *Front Endocrinol (Lausanne)*. 2021;12:676403-676416.
33. Bretones G, Delgado MD, Leon J. Myc and cell cycle control. *Biochim Biophys Acta*. 2015;1849(5):506-516.
34. Spangrude GJ, Heimfeld S, Weissman IL. Purification and characterization of mouse hematopoietic stem cells. *Science*. 1988;241(4861):58-62.
35. Kiel MJ, Yilmaz OH, Iwashita T, Yilmaz OH, Terhorst C, Morrison SJ. SLAM family receptors distinguish hematopoietic stem and progenitor cells and reveal endothelial niches for stem cells. *Cell*. 2005;121(7):1109-1121.
36. Gekas C, Graf T. CD41 expression marks myeloid-biased adult hematopoietic stem cells and increases with age. *Blood*. 2013;121(22):4463-4472.
37. Bernitz JM, Daniel MG, Fstkchyan YS, Moore K. Granulocyte colony-stimulating

factor mobilizes dormant hematopoietic stem cells without proliferation in mice. *Blood*. 2017;129(14):1901-1912.

38. Grisouard J, Shimizu T, Duek A, et al. Deletion of Stat3 in hematopoietic cells enhances thrombocytosis and shortens survival in a JAK2-V617F mouse model of MPN. *Blood*. 2015;125(13):2131-2140.

39. Taniguchi Ishikawa E, Chang KH, Nayak R, et al. Klf5 controls bone marrow homing of stem cells and progenitors through Rab5-mediated beta1/beta2-integrin trafficking. *Nat Commun*. 2013;4:1660-1672.

40. Zhang Y, Xue Y, Cao C, et al. Thyroid hormone regulates hematopoiesis via the TR-KLF9 axis. *Blood*. 2017;130(20):2161-2170.

41. Ekblom M. Expression of spectrin in normal and malignant erythropoiesis. *Scand J Haematol*. 1984;33(4):378-385.

42. Takubo K, Nagamatsu G, Kobayashi CI, et al. Regulation of glycolysis by Pdk functions as a metabolic checkpoint for cell cycle quiescence in hematopoietic stem cells. *Cell Stem Cell*. 2013;12(1):49-61.

43. Flohr Svendsen A, Yang D, Kim K, et al. A comprehensive transcriptome signature of murine hematopoietic stem cell aging. *Blood*. 2021;138(6):439-451.

44. Kim J, Lee JH, Iyer VR. Global identification of Myc target genes reveals its direct role in mitochondrial biogenesis and its E-box usage in vivo. *PLoS One*. 2008;3(3):e1798-e1810.

45. Fenix AM, Miyaoka Y, Bertero A, et al. Gain-of-function cardiomyopathic mutations in RBM20 rewire splicing regulation and re-distribute ribonucleoprotein granules within processing bodies. *Nat Commun*. 2021;12(1):6324-6338.

46. Itskovich SS, Gurunathan A, Clark J, et al. MBNL1 regulates essential alternative RNA splicing patterns in MLL-rearranged leukemia. *Nat Commun*. 2020;11(1):2369-2383.

47. Ciau-Uitz A, Wang L, Patient R, Liu F. ETS transcription factors in hematopoietic stem cell development. *Blood Cells Mol Dis*. 2013;51(4):248-255.

48. Gilmour J, O'Connor L, Middleton CP, et al. Robust hematopoietic specification requires the ubiquitous Sp1 and Sp3 transcription factors. *Epigenetics Chromatin*. 2019;12(1):33-52.

49. Liu Y, Chen Y, Deng X, Zhou J. ATF3 prevents stress-induced hematopoietic stem cell exhaustion. *Front Cell Dev Biol*. 2020;8:585771-585780.

50. Gao J, Chen YH, Peterson LC. GATA family transcriptional factors: emerging suspects in hematologic disorders. *Exp Hematol Oncol*. 2015;4:28-35.

51. Nottingham WT, Jarratt A, Burgess M, et al. Runx1-mediated hematopoietic stem-cell emergence is controlled by a Gata/Ets/SCL-regulated enhancer. *Blood*. 2007;110(13):4188-4197.

52. Unnisa Z, Clark JP, Roychoudhury J, et al. Meis1 preserves hematopoietic stem cells in mice by limiting oxidative stress. *Blood*. 2012;120(25):4973-4981.

53. Burda P, Laslo P, Stopka T. The role of PU.1 and GATA-1 transcription factors during normal and leukemogenic hematopoiesis. *Leukemia*. 2010;24(7):1249-1257.

54. Cabal-Hierro L, van Galen P, Prado MA, et al. Chromatin accessibility promotes hematopoietic and leukemia stem cell activity. *Nat Commun*. 2020;11(1):1406-1424.

55. Swygert SG, Kim S, Wu X, et al. Condensin-dependent chromatin compaction represses transcription globally during quiescence. *Mol Cell*. 2019;73(3):533-546.e534.

56. Sheng Y, Ma R, Yu C, et al. Role of c-Myc haploinsufficiency in the maintenance of HSCs in mice. *Blood*. 2021;137(5):610-623.

57. Cheng Y, Luo H, Izzo F, et al. m(6)A RNA methylation maintains hematopoietic stem cell identity and symmetric commitment. *Cell Rep*. 2019;28(7):1703-1716.e1706.

58. Althoff MJ, Nayak RC, Hegde S, et al. Yap1-Scribble polarization is required for hematopoietic stem cell division and fate. *Blood*. 2020;136(16):1824-1836.

59. Mullally A, Lane SW, Ball B, et al. Physiological Jak2V617F expression causes a lethal myeloproliferative neoplasm with differential effects on hematopoietic stem and progenitor cells. *Cancer Cell*. 2010;17(6):584-596.

60. De Bosscher K, Desmet SJ, Clarisse D, Estebanez-Perpina E, Brunsveld L. Nuclear receptor crosstalk - defining the mechanisms for therapeutic innovation. *Nat Rev Endocrinol*. 2020;16(7):363-377.

61. Di Martino O, Niu H, Hadwiger G, et al. Endogenous and combination retinoids are active in myelomonocytic leukemias. *Haematologica*. 2021;106(4):1008-1021.

62. Niu H, Fujiwara H, di Martino O, et al. Endogenous retinoid X receptor ligands in mouse hematopoietic cells. *Sci Signal*. 2017;10(503):eaan1011-eaan1037.

63. Dong S, Wang Q, Kao YR, et al. Chaperone-mediated autophagy sustains haematopoietic stem-cell function. *Nature*. 2021;591(7848):117-123.

64. Canete A, Cano E, Munoz-Chapuli R, Carmona R. Role of Vitamin A/retinoic acid in regulation of embryonic and adult hematopoiesis. *Nutrients*. 2017;9(2):159-177.

65. Wilson A, Murphy MJ, Oskarsson T, et al. c-Myc controls the balance between hematopoietic stem cell self-renewal and differentiation. *Genes Dev*. 2004;18(22):2747-2763.

66. Hsu TY, Simon LM, Neill NJ, et al. The spliceosome is a therapeutic vulnerability in MYC-driven cancer. *Nature*. 2015;525(7569):384-388.

67. Anczukow O, Krainer AR. The spliceosome, a potential Achilles heel of MYC-driven tumors. *Genome Med*. 2015;7:107-111.

68. Adelman ER, Huang HT, Roisman A, et al. Aging human hematopoietic stem cells manifest profound epigenetic reprogramming of enhancers that may predispose to leukemia. *Cancer Discov*. 2019;9(8):1080-1101.

69. Yoshida K, Sanada M, Shiraishi Y, et al. Frequent pathway mutations of splicing machinery in myelodysplasia. *Nature*. 2011;478(7367):64-69.

70. Venkatasubramanian M, Chen X, Kashish Chetal M, et al. A prognostic human splicing signature that precurses leukemia. *Blood*. 2018;132(suppl 1):877-880.

71. Chen H, Liu H, Qing G. Targeting oncogenic Myc as a strategy for cancer treatment. *Signal Transduct Target Ther*. 2018;3:5-12.